2015

Dynamic Penetration of a Flying Wing Anchor in Sand in Relation to Floating Offshore Wind Turbines

Nikolaus Benedikt Breithaupt
University of Rhode Island, bbreithaupt@my.uri.edu

DYNAMIC PENETRATION OF A FLYING WING ANCHOR IN SAND IN RELATION TO FLOATING OFFSHORE WIND TURBINES

BY

NIKOLAUS BENEDIKT BREITHAUPT

A THESIS SUBMITTED IN PARTIAL FULFILLMENT OF THE

REQUIREMENTS FOR THE DEGREE OF

MASTER OF SCIENCE

IN

CIVIL AND ENVIRONMENTAL ENGINEERING

UNIVERSITY OF RHODE ISLAND

2015

MASTER OF SCIENCE THESIS

OF

NIKOLAUS BENEDIKT BREITHAUPT

APPROVED:

Thesis Committee:

Major Professor Aaron S. Bradshaw

Christopher D.P. Baxter

David Taggart

Nasser H. Zawia
DEAN OF THE GRADUATE SCHOOL

UNIVERSITY OF RHODE ISLAND
2015

ABSTRACT

A new concept called the Flying Wing Anchor was recently proposed that consists of a kite-shaped plate anchor that is installed by free-fall penetration, and then rotates into a position that is near normal to the mooring line. Understanding the free-fall penetration behavior and initial embedment depth is critical to assessing the feasibility of the anchor in sandy soils. Small-scale 1g model tests were performed to investigate the dynamic penetration behavior of the anchor both in dry and saturated sand. Simple numerical models were also developed to model the dynamic penetration under drained and undrained conditions. The results indicated that dynamic penetration is likely an undrained process and the key factor controlling the embedment is the undrained strength and strain rate effects. Considering an undrained loading it may be possible for the Flying Wind Anchor to achieve embedment depths of up to 3 times the anchor height in loose sands.

ACKNOWLEDGEMENTS

The past year has been one of the most interesting years in my life. People on so many levels have influenced my life in a personally as well as a professional way.

First of all, this thesis would not have been possible without my Major Professor, Dr. Aaron Bradshaw, for his support, inspiration, and pure enthusiasm throughout my research. I am truly grateful for the support during my masters at University of Rhode Island.

In addition, I would like to thank Dr. Christopher Baxter for his input and assistance toward my research and for providing me knowledge and insight throughout my graduate studies. I want to extend my gratitude to Joe Giampa for his help and input towards this research. I feel very thankful to everyone who has been supporting my studies and contributed to it in any way.

Lastly, thank you to my amazingly supportive and loving family, my parents Andreas and Monika as well as my sisters Clara and Johanna. You have always been there and helped me to strive to be the best I can be through every aspect of life. If it was not for you I would not be the person I am today.

TABLE OF CONTENTS

LIST OF TABLES

LIST OF FIGURES

CHAPTER 1: INTRODUCTION

Chapter 1 introduces into the topic of Flying Wing Anchors (patent pending) and gives background of this research. Further, the statement of the problem and the objectives of this study will be introduced.

INTRODUCTION AND BACKGROUND

Global energy consumption is constantly increasing. Modern societies, politics and economy are facing the problem of how to satisfy the need for a permanent and sustainable energy supply. One possible solution is to increase offshore wind energy production. Studies by Musial & Butterfield (2004) have shown that the overall offshore wind energy resources of the United States are 908,000 MW.

While offshore wind turbines in shallow water depth are already widely distributed in Europe, there is still a lack of deep-water solutions due to technical and economic issues as well as practical experience. Nevertheless, wind power in general has developed itself as a major source of renewable energy. Furthermore, onshore wind farms have satisfied the large demand for electricity in the United States and Europe (Matha et al., 2009).

Studies by Musial & Butterfield (2004) have shown that only 10 % of the US offshore wind energy resources are located in shallow waters, up to 30 m in depth. The larger part, 90%, of the US offshore wind energy resources is located in deep water with depths of more than 30 m. For New England the overall offshore wind energy resources are 220,500 MW, where almost 95% are located in deep water.

The general difficulties of offshore wind turbines are high investment costs, higher capital and maintenance costs, as well as the different environmental conditions at sea such as more corrosion from salt water, additional loads from waves and ice and obviously higher construction cost. These difficulties require a long planning phase including environmental, engineering, feasibility and site-specific studies (Breton and Moe, 2009).

Currently the majority of wind farms in the world are located either in shallow water or onshore. Shallow water depths allow the manufacturers to use conventional land-based turbines with upgraded electrical and corrosion control systems. These fixed-bottom structures are placed on a foundation in the seabed and are, therefore, limited to water depths of about 30 m.

Therefore, there is a need to develop new technologies for deep-water foundations, because fixed-bottom systems, such as lattice-jacket and tripods are not practical in greater water depths (Butterfield et al., 2007). Floating options are being investigated for such cases for which the load would be carried by the buoyancy force. In this regard, experience developed in the offshore oil and gas industry in countries like Norway, the US and UK could be highly valuable (Breton and Moe, 2009).

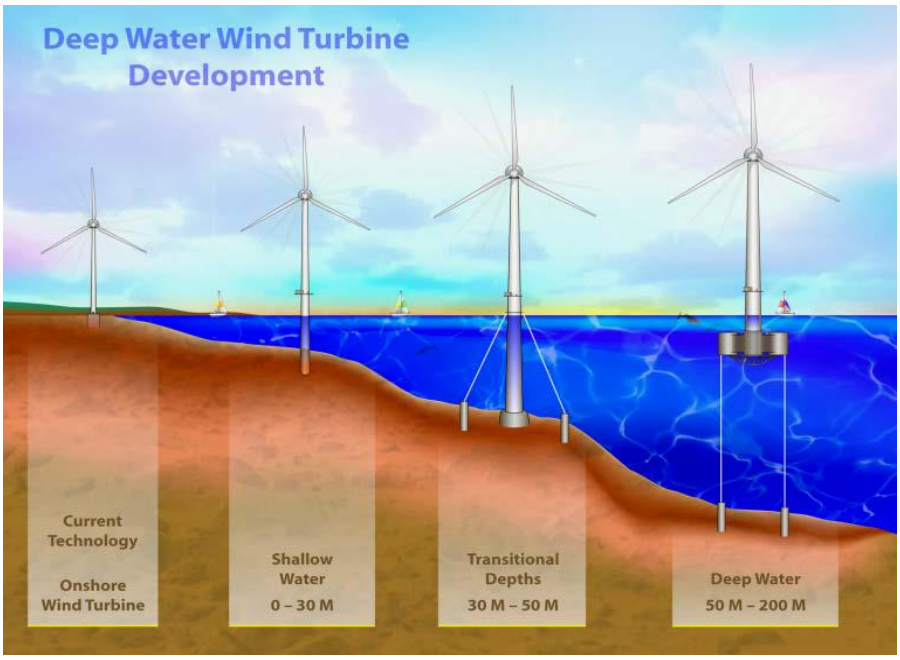

Figure 1: Progression of Expected Wind Turbine Evolution to Deeper Water (Musial & Butterfield, 2004)

A new "green" anchor concept called the Flying Wing Anchor (patent pending) was proposed by Gilbert and Bradshaw (2012) for floating offshore wind platforms. The Flying Wing Anchor is a combination of a torpedo pile anchor and a plate anchor. The anchor is lowered into the water by a long chain or cable and dropped from above the sea floor with its nose facing down thereby penetrating vertically the soil like a torpedo anchor. By increasing the mooring line tension the anchor moves along a specific trajectory until it reaches the expected soil depth at a certain orientation like a plate anchor (Figure 2).

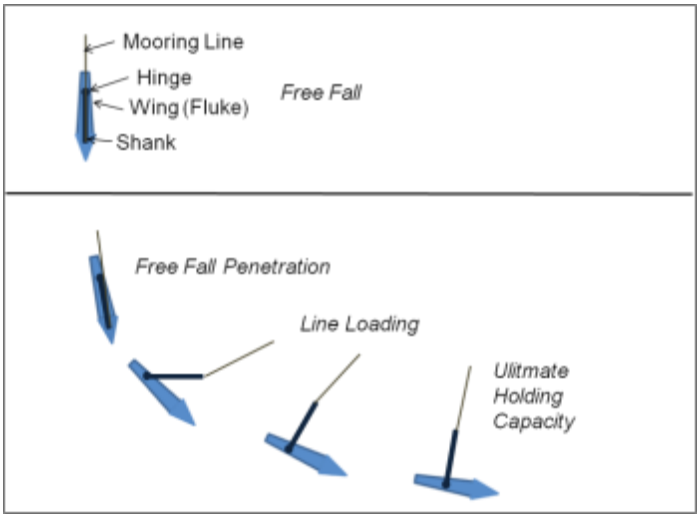

Figure 2: Flying Wing Anchor (patent pending) during penetration and loading (Gilbert and Bradshaw, 2012)

The Flying Wing Anchor is a new concept that needs further research. However, preliminary analyses and model tests executed by University of Texas and University of Rhode Island show promise for this concept. The anchor has the potential to be used in many different applications, such as foundation for offshore wind turbines, floating bridges and renewable energy power plants for waves. Although the concept seems feasible, a fundamental understanding of the soil-structure interaction that considers the orders-of-magnitude range of shear rates during free-fall penetration, line pre-tensioning and environmental loading in practice needs to be further investigated.

Research on the Flying Wing Anchor in clays is currently being performed at the University of Texas (UT), University College Dublin (UCD), and Queens University Belfast (QUB). UT is performing 1g model testing of the anchor in clay soils along with analytical modeling of the anchor kinematics. UCD is performing detailed numerical

analyses of the anchor capacity in clay. QUB is investigating the strength of clays at very high rates of strain that might be achieved during free-fall penetration.

Research on the Flying Wing Anchor in sands is ongoing at the University of Rhode Island. The research approach has been to look at the three phases of anchor installation and service loading including (1) free-fall penetration, (2) trajectory, and (3) capacity. Studies of anchor capacity were initiated by Dietrich (2014) and trajectory is currently being investigated by Sivarajah (2015). This thesis focuses on the free-fall penetration aspects of the Flying Wing Anchor in sand.

STATEMENT OF THE PROBLEM

Although dynamically penetrating anchors in general have been studied in clay, there is very little information available to support the feasibility of installing dynamically penetrating anchors in sand. Based on the literature, dynamic penetration has been studied mainly for torpedo-type anchors in calcareous sands. There is essentially no data on the dynamic penetration of plate-shaped anchors in sands in general.

OBJECTIVES OF THIS STUDY

The objective of this study is to investigate and analyze the behavior of a new anchor concept called the Flying Wing Anchor under free-fall penetration in sand. This will be accomplished through a combination of 1g model experiments and numerical modeling.

CHAPTER 2: LITERATURE REVIEW

This chapter summarizes the existing literature related to dynamically penetrating anchors in sands.

DEEP PENETRATING ANCHORS AND TORPEDO PILES

Some research has already been done on dynamically penetrating anchors. One example is the Deep Penetrating Anchors (DPA) first introduced by Lieng et al. (1999). DPAs are rocket-shaped anchors, which when released from a specified height above the seabed, free-fall through the water and penetrate the ocean floor.

In the category of DPAs, Medeiros (2001) first introduced the concept of "Torpedo" piles. This anchor system consists of a pipe pile filled with scrap chain and concrete, close ended with a cone tip and is installed by free fall from a vessel.

Medeiros (2002) tested the penetration of torpedo piles in sands in Brazil. To evaluate the torpedo pile penetration, computer programs were developed using the finite difference method and a viscoelasticplastic model to simulate the pile/soil interaction. Calculating the impact velocity and the maximum height from which to drop the torpedo, a computer program with hydrodynamic analysis was developed.

Figure 3: Torpedo with Fins and Top Padeye used by Medeiros (2002)

In practice, the impact velocities of the torpedo piles varied between 10 to 22 m/sec, with free fall heights from 30 m to 150 m. The pile penetration in normally consolidated clay varied from 8 m to 22 m (top position after driving). The test results further show that from a drop height of 30 m the medium pile penetrations were:

- 29 m in normally consolidated clay;
- 13.5 m in over consolidated clay;
- 15 m in uncemented calcareous sand;
- 22 m in a seabed soil with a first 13 m thick fine sand layer and an adjacent normally consolidated clay layer

For 30-inch diameter piles, with a medium penetration of 20 m, the ultimate resistance after driving in horizontal direction varied between 900 to 1100 kN, ten days later the piles failed under 1700 kN to 2200 kN. For the 42-inch diameter piles, loads were applied at an angle of 45 degrees. After driving, with medium penetration of 29 m, the piles failed due to loads of 1900 kN to 2100 kN, later with a medium load of 3950 kN after 18

days. In pull out tests, the medium soil resistance was about 800 kN and after 10 days the piles failed with loads between 2000 to 2200 kN.

The authors further summarize that torpedo piles are less sensitive to increasing water depth than conventional concepts, because special subsea equipment or large support vessels are not required.

Richardson et al. (2005) carried out research where they analyzed the behavior of DPAs in calcareous sand through a series of centrifuge model tests (see Figure 4). As a model anchor, Richardson et al. (2005) used a 1:200 scale model, fabricated from brass and designed in accordance with the Type I Torpedo Anchor reported by Medeiros (2001). The purpose of their research was to predict embedment depth from the impact velocity.

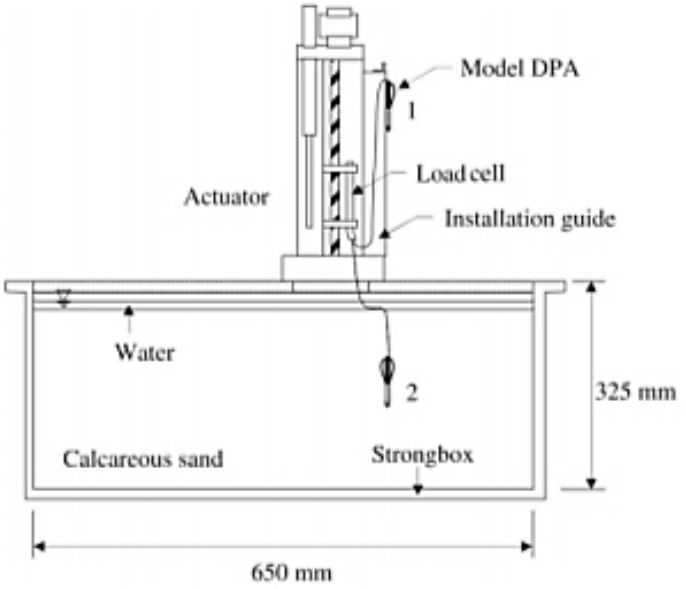

Figure 4: Centrifuge test setup used by Richardson et al. (2005)

Richardson et al. (2005) proposed the following equation to predict the vertical pullout capacity:

$$F_v = W_s + N_q \sigma_v' A_p + \beta \sigma_v' A_{shaft} \quad (1)$$

Where F_v is the vertical pullout capacity, W_s is the submerged anchor weight, N_q is the bearing capacity factor, σ_v' is the vertical effective stress, A_p is the projected area of the anchor, β is the ratio of shaft friction to effective overburden stress and A_{shaft} is the shaft area of the anchor.

In addition to the vertical pullout capacity formula, Richardson et al. (2005) also found expressions for the static resistance force F_s.

$$F_s = N_q \sigma_v' A_p + \beta \sigma_v' A_{shaft} \quad (2)$$

Furthermore, the equation of motion for anchors were introduced.

$$m \frac{d^2 z}{dt^2} = W_s - R_f \left(N_q \sigma_v' A_p + \beta \sigma_v' A_{shaft} \right) \quad (3)$$

where m is the anchor mass and R_f is a rate dependent term to account for velocity dependence of the soil resistance terms. R_f is further defined as:

$$R_f = (1 + \lambda \log \frac{v}{v_s}) \quad (4)$$

Where λ is a constant, v is the anchor velocity and v_s is the reference penetration velocity at which the static resistance was measured (1 mm/s). A finite difference approach was used to solve Equation 3.

Richardson et al. (2005) stated that the bearing capacity factor N_q as well as the ratio β in calcareous sand is somewhat uncertain, therefore the β has been applied to fit the

measured static pullout capacity data. The authors used N_q values of 32 and 35 with β values of 0.42 and 0.3. The average value of λ = 0.006, which are 0.6% per log cycle.

Overall, Richardson et al. (2005) indicated that the DPA has potential as an anchoring system in calcareous sediments. Additionally, with the given formulas it is possible to predict the embedment in calcareous sand from the static resistance profile. Embedment depths of around one times the fluke length were reported for tests with an impact velocity of 20 to 25 m/s.

Raie and Tassoulas (2009) present a procedure for computational modeling of a torpedo anchor penetrating into the soil. The procedure uses a Computational Fluid Dynamics (CFD) model to evaluate resisting forces on the anchor. The CFD approach, which represents soil as a viscous fluid, can be used for predictions of the embedment depth and further to provide estimates of the pressure and distributions in the soil. The CFD model is further capable of simulating the installation of the pile from the transition of the anchor from the water into the soil. Moreover, it predicts embedment depth and shear distributions along the anchor and in the soil. The authors use the computer program FLUENT, which is based on the finite-volume method. The soil is modelled as non-Newtonian Bingham fluid with shear thinning (pseudoplastic). The shear stress is defined as:

$$\tau = \tau_0 + \kappa(\dot{\gamma}^n - \dot{\gamma}_0^n), for\ \dot{\gamma} > \dot{\gamma}_0 \quad (5)$$

$$\tau = \mu_0 * \dot{\gamma}, for\ \dot{\gamma} \leq \dot{\gamma}_0 \quad (6)$$

Where τ and τ_0 are shear stress and yield shear stress, $\dot{\gamma}$ is the shear strain rate, $\dot{\gamma}_0$is the yield shear strain rate, κ is the consistency index, n is the power-law and μ_0 is the yield viscosity that is defined as the yield shear stress over the yield shear strain rate. At the tip of the shaft, an ad hoc increase is assumed. This increase is defined as

$$\tau_{0,tip} = \frac{1}{\pi} * \frac{A_F}{A_T} * N_c * S_u \quad (7)$$

$\tau_{0,tip}$ is the yield shear stress specified at the tip, S_u is the static undrained shear strength of the soil, N_c is the end-bearing factor. A_F and A_T are the penetrator frontal area and projected area of the tip on the plane parallel to the penetrator longitudinal axis.

The CFD procedure gave promising results in predicting the embedment depth in both a laboratory and full-scale torpedo anchor installation tests in clays. In the CFD procedure, there is no further need to assume the anchor effective mass, internal drag force and side adhesion factor as the case in the analytical approach. Additionally, it provides estimates of the pressure and shear distributions on the soil-anchor interface and in the soil.

Embedment depth from dynamically penetrating objects under undrained conditions has also been discussed in the Handbook for Marine Geotechnical Engineering (2011). Under dynamic penetration, the authors define velocities between 1 m/s and 122 m/s. The forces acting on the penetrating object are shown in the formula below, where a positive force describes a downward and a negative force describes a resisting or upward force.

$$F_i = F_{di} + W_{bi} - Q_{ni} - F_{si} - F_{hi} \quad (8)$$

Where F_i is the net total downward force, F_{di} is the external driving force (e.g. rocket motor), W_{bi} is the penetrator buoyant weight, Q_{ni} is the nose or tip bearing resistance, F_{si}

is the side friction or adhesion and F_{hi} is the fluid drag force. Figure 5 shows the forces acting on the penetrator before and after contact with the seafloor.

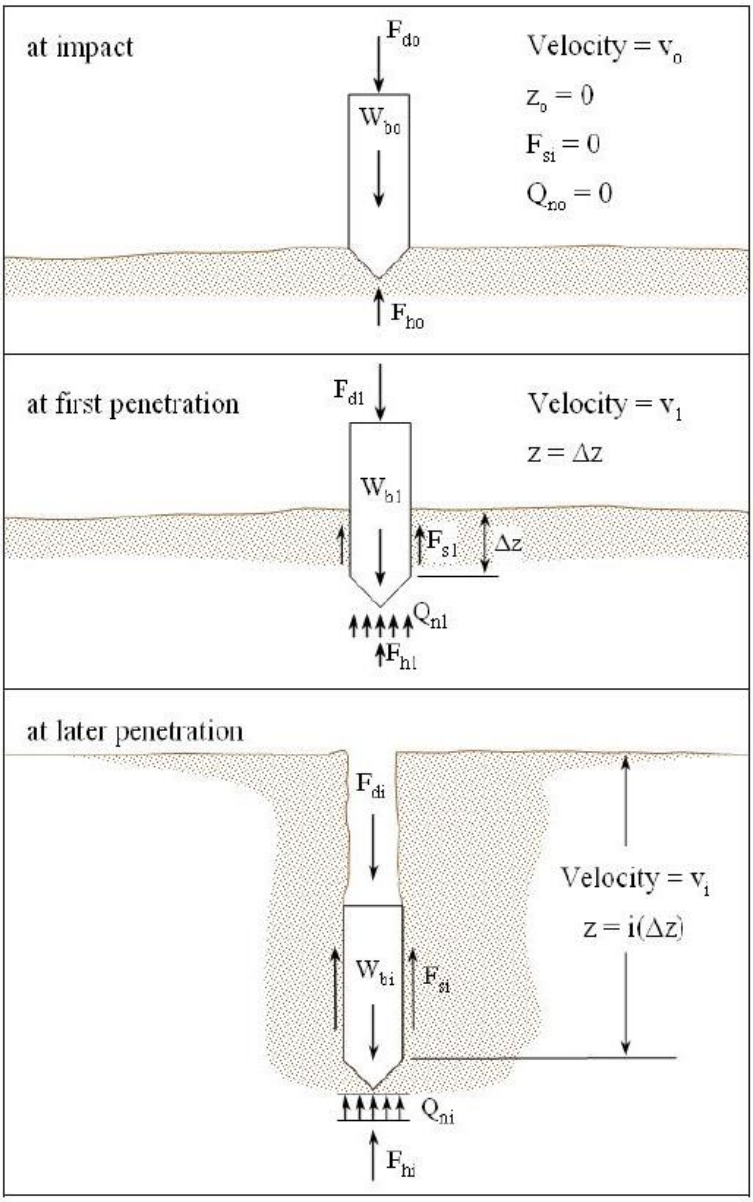

Figure 5: Forces acting on the Penetrator before and after contact with the Seafloor (NAVFAC, 2011)

The tip resistance can be determined as

$$Q_{ni} = S_{ui}(nose) S_{\dot{e}\imath} N_{ti} A_t \quad (9)$$

Where $S_{ui}(nose)$ is the soil undrained shear strength at a depth 0.35 B below z, averaged over ith increment of penetration, $S_{\dot{e}\imath}$ is the strain rate factor, A_t is the end area of penetrator and N_{ti} is a dimensionless nose resistance factor, which is determined by the following formula.

$$N_{ti} = N_c' = [(2+\pi)]\left[1+\left(\frac{1}{2+\pi}\right)\left(\frac{B}{L}\right)\right][1+\left(\frac{2}{2+\pi}\right)\arctan\left(\frac{D_f}{B}\right)] \quad (10)$$

The soil undrained shear strength is determined from the following equation based on the work of Seed and Lee (1967):

$$S_{ui}(nose) = \left[\frac{\sigma_{cr}\left(N_\phi - 1\right)}{2}\right] \quad (11)$$

Where σ_{cr} is the critical confining stress, and N_ϕ is a bearing factor. The critical confining stress σ_{cr} is estimated with the formula:

$$\sigma_{cr} = {D_r}^{1.7} * 958\ kPa \quad (12)$$

Where D_r is the fractional relative density calculated by the following equation:

$$D_r = \left(\gamma_b - 8.9\ {kN}/{m^3}\right)/1.8\,{kN}/{m^3} \quad (13)$$

The bearing factor N_ϕ is determined by:

$$N_\phi = \tan^2\left(45^\circ + \frac{\phi}{2}\right) \quad (14)$$

The side friction F_{si} is determined with

$$F_{si} = \left[\frac{S_{ui}\,(side)}{S_{ti}}\right] S_{\dot{e}\imath} A_{si} \quad (15)$$

Where S_{ui} is the soil undrained shear strength averaged over the length of the penetrator in contact with the soil, A_{si} is the side soil contact area of the penetrator, S_{ti} is the soil sensitivity.

$$S_{\dot{e}i} = \frac{S_{\dot{e}}^*}{1 + [\frac{C_{\dot{e}} v_i}{s_{ui} D_e} + C_0]^{-0.5}} \tag{16}$$

Where $S_{\dot{e}}^*$ is the maximum strain rate factor, $C_{\dot{e}}$ is the empirical strain rate coefficient, v_i is the velocity at a certain depth, C_0 is the empirical strain rate constant, s_{ui} is the undrained shear strength and D_e is the equivalent diameter of penetrator.

The fluid drag force is acting while moving through water, hence, it is further assumed that this force is also existing when the object is penetrating into the soil. This force is calculated by the following formula:

$$F_{hi} = (0.5) C_D \rho A_t (v_i)^2 \tag{17}$$

Where C_D is the dimensionless fluid drag coefficient, which is the same as that in seawater, ρ is the mass density of the soil, the "fluid" being accelerated and v_i is the penetrator velocity after penetrating the ith layer.

The inertial force is defined as the following:

$$F_i = M v_i \left(\frac{dv}{dz}\right) \tag{18}$$

Where M is the penetrator mass and the ratio is describing the instantaneous change in velocity. In the following, the ratio should be replaced by $(2\Delta v)/(2\Delta z)$. The double increments are used to minimize deviations in the prediction.

$$2\Delta v = \frac{2\Delta z}{M}\left(\frac{F_i}{v_i}\right) \tag{19}$$

The new velocity increment for (i+1)th increment is given by:

$$v_{i+1} = v_{i-1} + 2\Delta v_i \tag{20}$$

For the incremental calculation, the velocity at i=1 needs to be defined as

$$v_1 = v_0 + \left(\frac{1}{v_0}\right)\left[\left(\frac{\Delta z}{M}\right)(F_{d.5} + W_{b.5} - Q_{n.5} - F_{s.5} - F_{h.5})\right] \tag{21}$$

Where $F_{d.5}, W_{b.5}, Q_{n.5}, F_{s.5}, F_{h.5}$ are initial estimates of the respective force values based on conditions at mid-depth in the first layer of penetration.

DYNAMICALLY EMBEDDED PLATE ANCHORS

The concept of Dynamically Embedded Plate Anchors (DEPLA) has been developed from the concept of Suction Embedded Plate Anchors (SEPLA). SEPLAs have been developed as an efficient anchoring system. This system combines the advantages of suction caissons, where the penetration depth and geographical location is known and vertically loaded plate anchors, which have a high geotechnical efficiency and low installation costs (Wilde et al., 2001). The concept was exclusively applied in clays.

The SEPLA consists basically of two parts, a suction caisson and a plate anchor, which is slotted vertically into its base. The suction caisson embeds the plate anchor and penetrates it into the seabed under self-weight. The water is pumped out of the interior of the caisson until it reaches the design embedment depth. In the following, the anchor mooring line is then disconnected from the caisson and the pump flow is reversed, which results in water being forced back into the caisson, causing the caisson to move upwards. In the meantime, the plate anchor is left in place at the designed depth. The mooring line,

which is attached to the plate anchor is then tensioned causing the plate anchor rotation in the ground to an orientation that is similar to the direction of the loading. (Gaudin et al., 2006) The installation process is also shown in Figure 6.

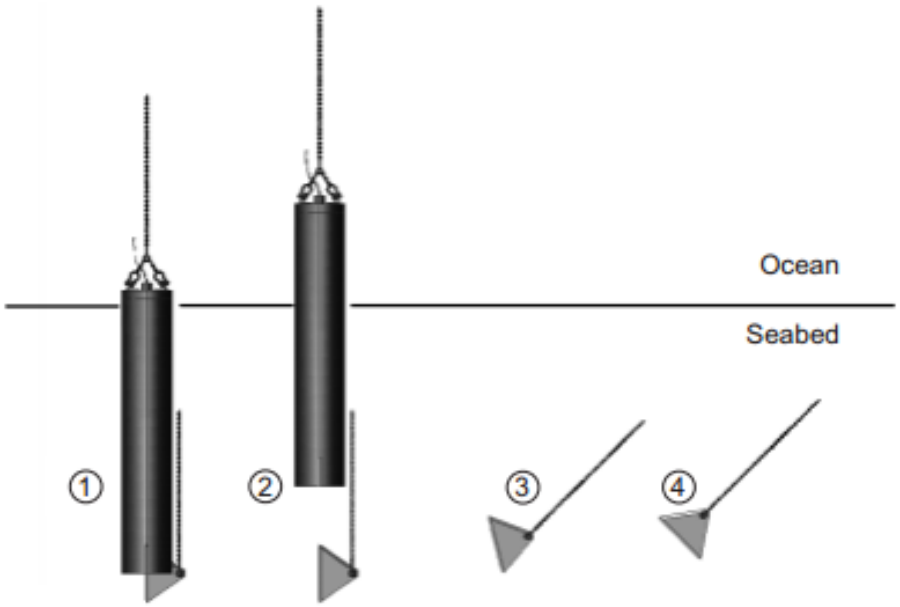

Figure 6: The SEPLA concept: 1, suction installation; 2, caisson retrieval; 3, anchor keying; 4, mobilised anchor (Gaudin et al. 2006)

With the increasing water depth, anchor installations become more time consuming and complex, which results in higher costs of construction. Due to the fact that no external energy source is needed, the DEPLA provides a more economical and sustainable solution than the SEPLA.

The anchor installation follows a similar approach like the SEPLA. A major difference is the DEPLA flukes and sleeves which will be relesed in the ground while the DEPLA follower will be pulled out and used for further anchor installations. Another difference is

that the anchor will be dropped from a certain height over the seabed. Therefore, the anchor is penetrating through water and later soil.

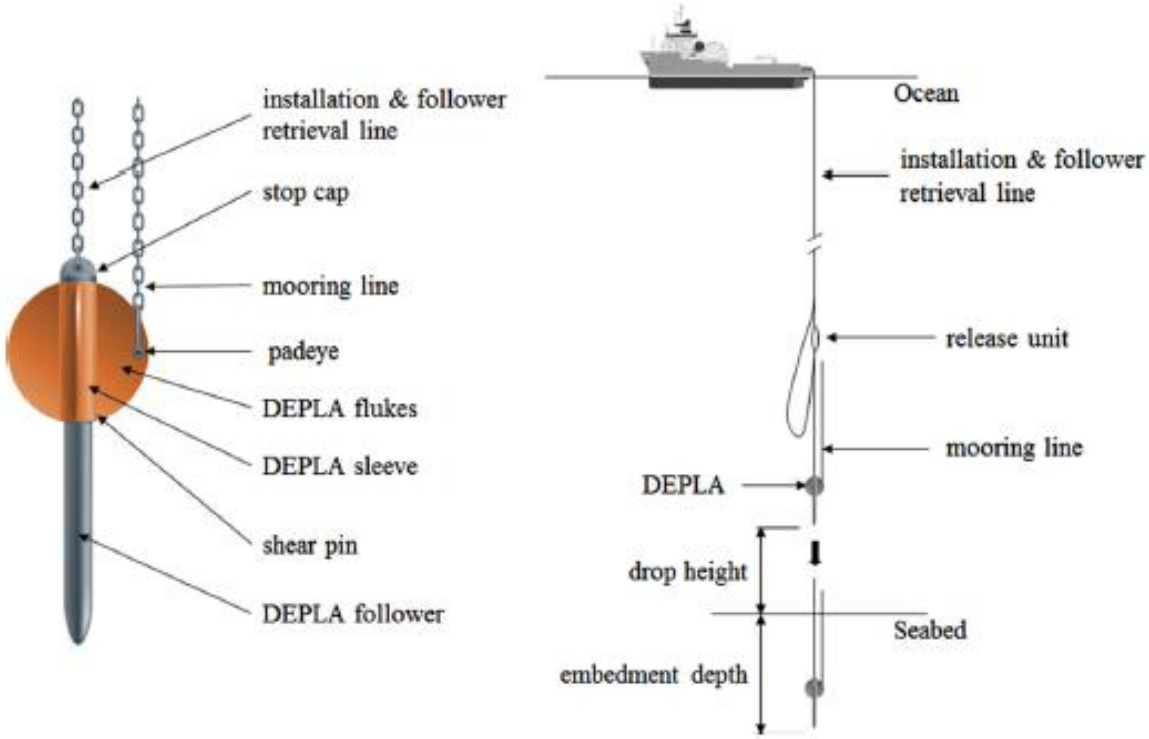

Figure 7: DEPLA (O'Loughlin et al., 2014)

Centrifuge studies by O'Loughlin et al. (2014) on DEPLA illustrated that the concept can work. Impact velocities of 27.5 to 30.0 m/s resulted in embedment depth of 1.6 to 2.8 times the length of the DEPLA follower. The majority of the test data was about 1.9 to 2.1 times the follower length, which shows respectively agreement with reported field test data of 1.9 to 2.4 times the anchor length for an anchor with a weight of 79 tons which is dynamically installed (Lieng et al., 2010).

CHAPTER 3: PHYSICAL MODELING METHODOLOGY

This chapter provides information on the methods used to perform small-scale physical modeling at 1g. The test anchors, test soil, static penetration tests, and dynamic penetration tests are described.

TEST ANCHORS

The test anchor geometry was obtained from the University of Texas. The anchor was designed to remain hydrodynamically stable during free-fall through the water column. The anchor had the following dimensions:

- Height of 105.9 mm
- Width of 127 mm
- Thickness of 12.7 mm

The geometry is shown in Figure 8.

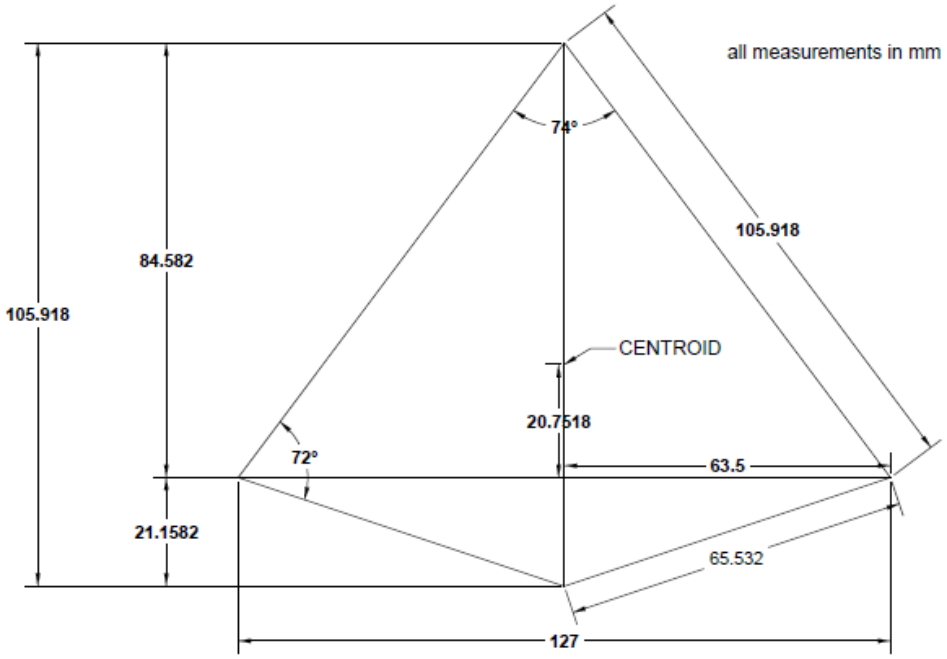

Figure 8: Anchor Shape with Dimensions

Two different test anchors were manufactured. Both anchors had the same dimensions, but differed in the design of the bottom section. The first one has an even bottom side (Figure 9), the other one is sharpened on both sides at an angle of 45 degrees (Figure 10 & 11).

Figure 9: Anchor Shape with blunt edge

Figure 10: Anchor Shape with sharp edge

Figure 11: Anchor Shape with sharp edge 2

The anchor could either be used with just a short rod, which should be simulating basically just the weight of the anchor or with the attached rod, which gives the possibility to add weight to the anchor (Figure 12). The length of the rod was designed in that way that a potential penetration under laboratory conditions would not exceed the length of the rod. In other words, the anchor would potentially stop before reaching the full length of the rod.

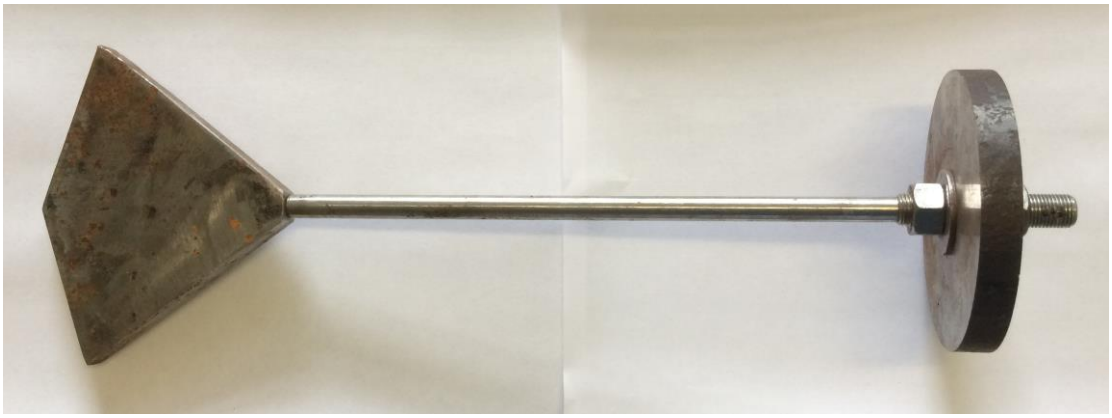

Figure 12: Anchor blunt edge with attached rod and added weight

The weights of the anchors were:

- 0.668 kg (1.473 lb) for the blunt-edged anchor
- 0.636 kg (1.403 lb) for the sharpened anchor

The small rod had a weight of 16.7 grams (0.037 lb); the large rod, seen in Figure 12, and the added weight summed up to 1.067 kg (2.354 lb). The total length of the anchor and rod is 39.4 cm (15.5 in).

TEST SOIL

Important for this study was the accurate determination of the soil and its properties. The soil used for the tests was obtained from Westerly, Rhode Island. The grain size distribution (Figure 13) suggests that the soil is uniform with sizes ranging from 0.2 – 1 mm and no fines.

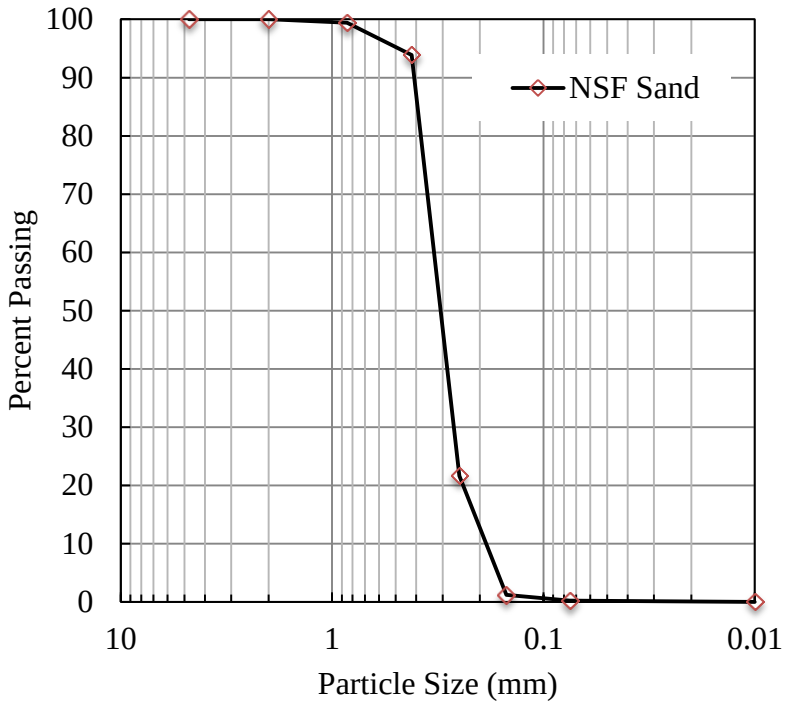

Figure 13: Grain size distribution of the test sand

The minimum and maximum dry unit weight were determined according to the procedures from ASTM D 4254 (Method C) and ASTM D 4253 (Method 1A) by Dietrich (2014). The following soil properties were determined:

Table 1: Soil properties of the Test sand

γ_{MAX} (kN/m³)	18.1
γ_{MIN} (kN/m³)	14.1
Φ'_{cs} (deg)	33.4
D_{50} (mm)	0.3
e_{MAX}	0.844
e_{MIN}	0.436
Cu	1.63
Cc	1.24
D_{60} (mm)	0.31
D_{10} (mm)	0.19
D_{30} (mm)	0.27

The static penetration tests were performed in a 0.9 m x 1.2 m x 2.4 m test tank and the in-place unit weight was determined by placing the cups of known volume at different heights within the tank. The average unit weight of the sample was 14.69 kN/m2. The relative density calculated with the following formula:

$$Dr\ (\gamma) = \frac{\gamma - \gamma_{MIN}}{\gamma_{MAX} - \gamma_{MIN}} \left(\frac{\gamma_{MAX}}{\gamma}\right) \quad (22)$$

The γ values are the dry unit weights from the test sample. γ_{MAX} and γ_{MIN} are taken from Table 1.

STATIC PENETRATION TESTS

TEST TANK

The test tank for static penetration tests was developed and was used before by the University of Rhode Island and had the following inside dimensions:

- Height: 0.914 m
- Width: 1.219 m
- Length: 2.413 m

The material for the sides and bottom was plywood reinforced by wooden beams. A second test tank with the same materials and dimensions was built alongside the one test tank but was mainly used as storage for the used sand.

Figure 14: Test Tank for static penetration tests; note the white cups measuring in-place unit weight

INSTRUMENTATION

Instrumentation for these tests included a string potentiometer for distance vs. time measurements, a load cell measuring the applied force and a Data Acquisition System (DAQ) was used to process the data. All these instruments are described in the following section.

A string potentiometer, often called a string pot, is a transducer which can detect and measure the linear position of an object. It is basically a long spool of nylon line attached to a transducer, which transforms the extent of the nylon cable into an electronic signal. The string pot we used was an SP2- 50 with a full stroke range of 1.27m (50 in) from the company Celesco (Figure 15).

Figure 15: Celesco String Potentiometer mounted on the frame

A load cell is a transducer which creates an electronic signal if a force, either tension or compression, is applied to it. The magnitude of the electronic signal is directly proportional to the applied force. In other words, the higher the force that is applied, the higher the signal that will be recognized by the Data Acquisition Tool (DAT). The load cell we used was a piezoelectric load cell SBA-500LB from the company Omega (Figure 16).

Figure 16: Load Cell Omega SBA-500LB

All sensor data was recorded using a Data Acquisition System (Figure 17). Through a data acquisition system, it is possible to record a signal from an external device (in this research: String pot and load cell). The signal in mV or V will be recorded and saved into an excel sheet. This excel sheet then contains the raw data which were recorded by the external devices. Later, this raw data can be used to process data and draw graphs. In addition to that, the Data Acquisition Tool we used had a power supply, which could provide small units with electricity. The Data Acquisition Tool was carefully chosen to fulfill both the requirements on precision of the data procession and the compatibility with the used devices. The Omega IstruNet 100 with a InstruNet 200 controller unit seem to fulfill these requirements best.

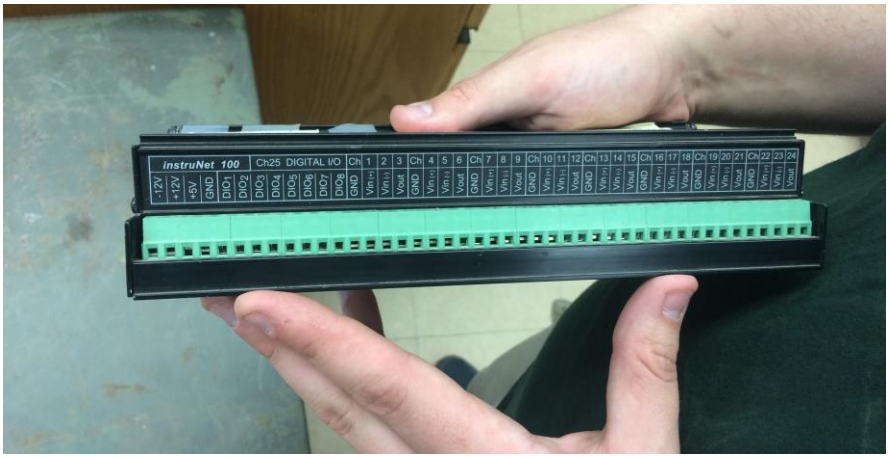

Figure 17: Data Acquisition System Omega InstruNet 100

SOIL PREPARATION

It was crucial for this research to have a uniform sand sample at a desired relative density. To achieve similar soil properties the concept of the pluviator was used. A portable pluviator developed by Dave and Dasaka (2012) and used by Gade et al. (2013) and Dietrich (2014) was seen to meet the requirements best (see Figure 18).

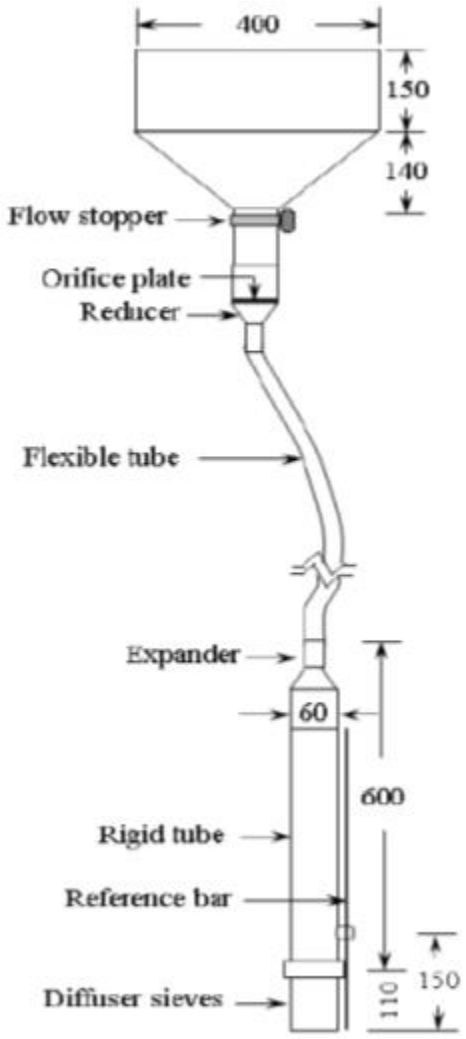

Figure 18: Details of Portable travelling pluviator assembly (Dave and Dasaka, 2012)

The concept of the portable pluviator was calibrated by varying drop height (50.8 mm to 190.5 mm) and the number of installed sieves to achieve a relative density of about 23 %. It was found out previously by Dietrich (2014) that a drop height of 152.4 mm and two 6.35 mm sieves resulted in a relative density of 23%.

For the dry tests the unit weights were varying from 14.81 kN/m³ to 15.22 kN/m³. The average unit weight throughout all dry samples was 14.97 kN/m³. The relative density for the dry tests varied between 22.0% and 33.0%, the average was at 26.0%.

TEST SET UP AND PROCEDURES

The test set up consisted of the test tank and a big frame over the test tank to mount equipment, such a as string potentiometer and a load cell. The dimensions of the test tank made it possible to run four tests at different positions without preparing a new sample. A schematic diagram is presented in Figure 19.

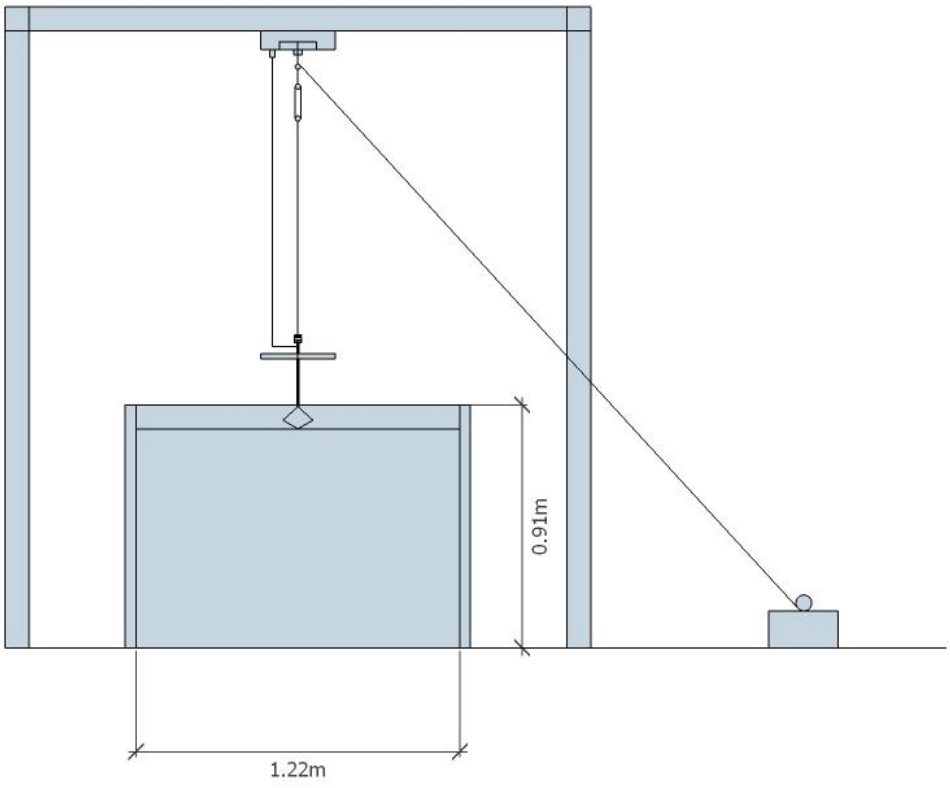

Figure 19: Schematic Diagram of Test Set Up for Static Penetration Tests

This test set up was used to run the static penetration test. The anchor is attached to the long rod and a load cell is screwed into the rod. The load cell is on the other side connected to a little rod on which weights could be added. This little rod is further connected to a long cable. The long cable is part of a winch which is attached to the ground. While the winch is releasing the cable the anchor with weight and load cell is going down and therefore the load cell is reading an increasing compression force. The anchor penetrates statically driven by the weight of anchor and added weight into the ground. This test was performed until a depth of around 2 – 3 anchor fluke length was reached.

Figure 20: Picture of Test Set Up for Static Penetration Test

A string potentiometer, described earlier, gives the extent of the cable and the data acquisition tool is giving the time. Therefore, it could be clearly seen at which point of time the string pot had which extent. A line can be drawn, showing which penetration at what point of time was achieved. Furthermore, this is especially crucial when comparing the sharpened anchor shape and the normal anchor shape.

In addition to that, the load being applied on the anchor was recorded by the load cell. This signal, which was sent by the load cell, could then be processed by the Data Acquisition Tool. Later the recorded data from the Data Acquisition Tool, which consisted of data from the string pot as well as the load cell, could be combined, which results in a force displacement relationship.

DYNAMIC PENETRATION TESTS

TEST TANK

The dynamic penetration test tank consisted of steel and was put on wheels which allowed it to be moved inside and outside, which was crucial for the high speed tests, which we ran in an outside environment. Furthermore, the test tank had the following dimensions:

- Height: 0.61 m (24 in)
- Inner diameter: 0.58 m (23 in)

The test tank was used for previous tests by the University of Rhode Island and was manufactured from steel, which made it possible to saturate the whole sample and simulate a saturated sand sample. Furthermore, the test tank can be dried after saturating it.

Figure 21: Test tank for dynamic penetration tests

SOIL PREPARATION

For the dry tests, the soil preparation was executed the same way as in the static penetration tests, which were described earlier. For the saturated sand sample, the tube was filled up to a height of 5 cm first, following the sand was pluviated first through the air and then through water. Great attention was paid to maintain a water level between 4 and 6 cm above the soil surface. This procedure was continued until the final volume of sand was reached. The water was maintained at a level of 4 to 6 cm above the soil surface. The soil sample rested for about two hours, then the water which remained over the soil surface was sucked from above till the water column over the soil column had dissipated.

For the saturated sand, the average total unit weight for the saturated sample was between 19.44 kN/m³ and 19.53 kN/m³. On average, the total unit weight of the saturated samples was 19.49 kN/m³. The dry unit weigh was between 15.38 kN/m³ and 15.42 kN/m³, on average 15.40 kN/m³. The relative density varied between 37.5% and 38.6%, on average at 38.1%.

TEST SET UP AND PROCEDURES

Figure 22 shows the test set up for the dynamic penetration test. This test set up was an inside test and built in the basement of the Bliss Hall at University of Rhode Island. A pulley was drilled in the ceiling of the basement. The pulley was frictionless or of low friction and, therefore, did not influence the experiment itself. The anchor was attached to a nylon line. This nylon line was strained from the ground to the anchor and, therefore, under tension. The height of the basement in Bliss Hall was 3.20 meters, which was the reason why the fall height was limited to the distance between test anchor and the upper edge of the test tank plus the test tank's upper edge to the soil surface in the test tank. By burning the nylon line the test could be started and the anchor fell down into the test tank without any friction neglecting air resistance.

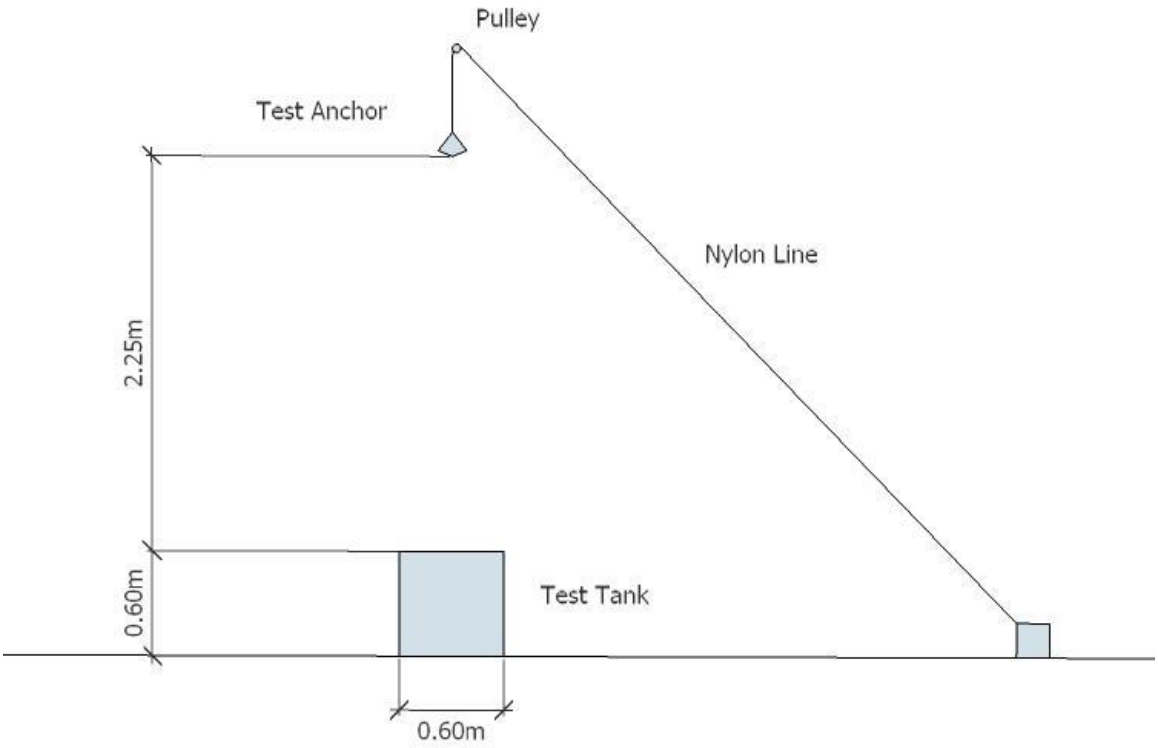

Figure 22: Test Set Up in Bliss Hall for dynamic penetration tests

In process of the research, a second test set up was developed. The test set up was basically moved outside to obtain a higher height by letting the anchor drop from the third story of an adjacent building.

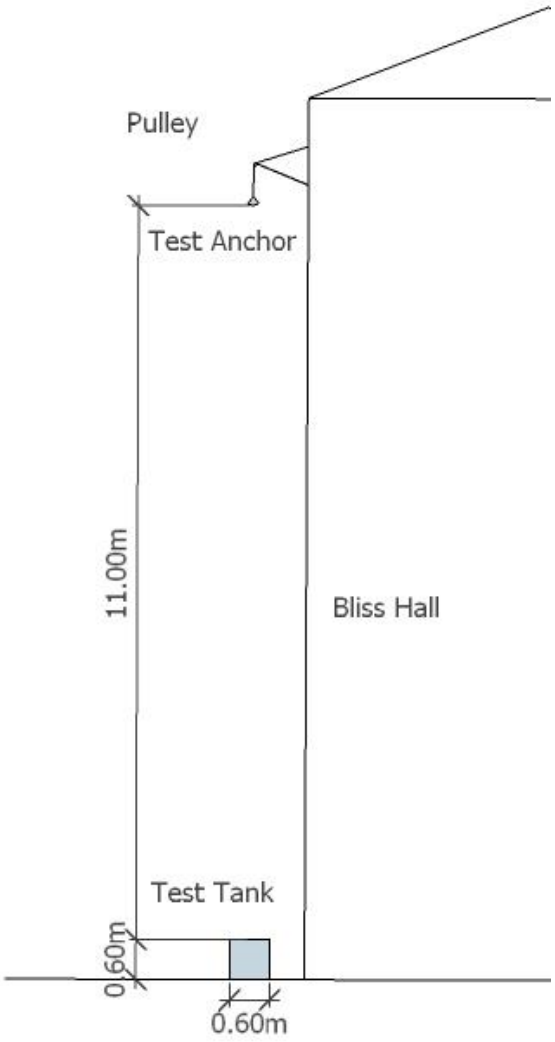

Figure 23: Test Set Up outside of Bliss Hall

The concept shown in Figure 23 is similar to the one inside the basement of Bliss Hall. In this case, the anchor was also attached to a nylon line, which was attached to a clamp inside the building. The height from the soil surface to the position of the anchor at the height of the third story of the building was 11 meters. The nylon line was burned the same way as in the inside test. Figure 24 shows a picture of the upper test set up, at the location where the anchor was attached, at the third story of Bliss Hall.

Figure 24: Test Set Up for the outside Tests. View on anchor and pulley

CHAPTER 4: PHYSICAL MODELING RESULTS AND DISCUSSION

This chapter presents the results and discussion of both the static and dynamic penetration tests described in Chapter 3.

STATIC PENETRATION TESTS IN DRY SAND

Figure 25 shows the applied load over the depth in the soil. Tests 1 and 2 had a blunt edge and Test 3 and 4 had a sharp edge (see also Chapter 3). In general, it can be said that Tests 1,2 and 4 behave in a similar way, while Test 3 seems to be off. In Test 3 the anchor tilted highly during penetration which highly affected the load cell and string pot readings. Test 3 was therefore excluded and retested by Test 4 which shows more likely what could be expected in terms of shape of the curve. Generally, Test 1,2 and 4 are penetrating under its own weight added by a constant force of around 15 N (read by load cell) to a depth of 30 mm (1.18 inches). After that, the curves are increasing more and from Figure 25 there appear to be significant differences between sharp and blunt edge, which will described in the following.

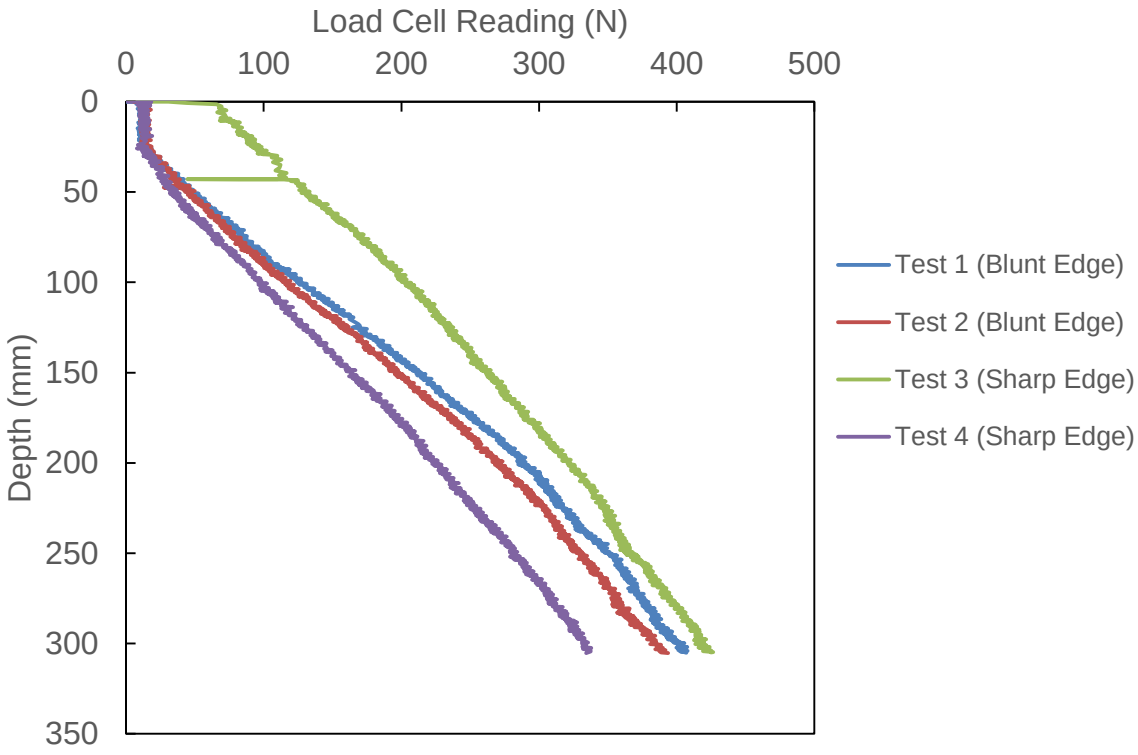

Figure 25: Depth vs. Load Cell Readings for the Static Penetration Tests

The blunt edge curves of Test 1 and 2 increase evenly after the first 30 mm where they appear rather constant. Furthermore, it can be stated that the curves of 1 and 2 are very similar in shape. At the greatest extent, both curves are off by around 20 N, which equals 5% using 380 N as a base. This underlines that both tests can display the behavior of the blunt edge anchor very well. As stated earlier, the anchors initially penetrate to a depth of 30 mm with a constant force of around 15 N. The plane shear of blunt edge shape anchors are then increasing slightly exponentially with the depth up to a point of around 155 N at a depth of 120 mm. Around that point, the increase is shrinking but still increasing to a depth of 300mm at a force of 390 N and 410 N.

The sharp edge curve (Test 4) also increases evenly after the first 30 mm with a constant force of around 15 N. The inclination can be described as linear and steady. An exponential increase at the beginning cannot be seen. At 140 N a depth of 150 mm is reached. The incline is shrinking slightly and hardly visible and remains at a steady increase until it reaches the final position at 300 mm in depth with a force of 335 N.

A difference between the sharp edge and the blunt edge is obvious. The bearing resistance is smaller and the applied force is less than for the blunt edge anchor at the same depth. The difference of the lines of sharp edge and blunt edge constantly increase until the final depth at 300 mm. The difference in the bearing stress is 35 kN/m2 at the max at final depth. Concluding, it can be stated that the sharp edge anchor is penetrating the soil more smoothly while the blunt edge anchor is displacing more soil due to the shape and, therefore, a higher applied load is necessary to reach the final depth of 300 mm.

Since the static push tests measure bearing capacity but also a small amount of side friction, a theoretical approach was taken in order to calculate the side resistance. Therefore K_0 was calculated with the formula, which is presented below:

$$K_0 = 1 - \sin\phi' \tag{24}$$

It has further been assumed that 1.5 * K_0 is equal to K, which is within the values from Conduto (2001) for driven piles. The friction angle in the test tank was assumed to be approximately 37 degrees based on triaxial data in Dietrich (2014). In addition to that, the horizontal stresses were calculated over the depth. The horizontal stress was calculated.

With the horizontal stress the bearing stress q_u could be calculated with the formula

$$q_u = Q_u / A_b \tag{25}$$

Where Q_u represents the measured toe force subtracted by the theoretical friction which was calculated with the horizontal stresses and A_b is the bearing area. The ratio of shaft resistance and toe resistance was calculated and revealed that this ratio was only 2.8% on average for the blunt edge and 3.4% for the sharp edge anchor.

The bearing stress q_u is plotted in Figure 26 for the three tests, which are two blunt edge and one sharp edge anchor.

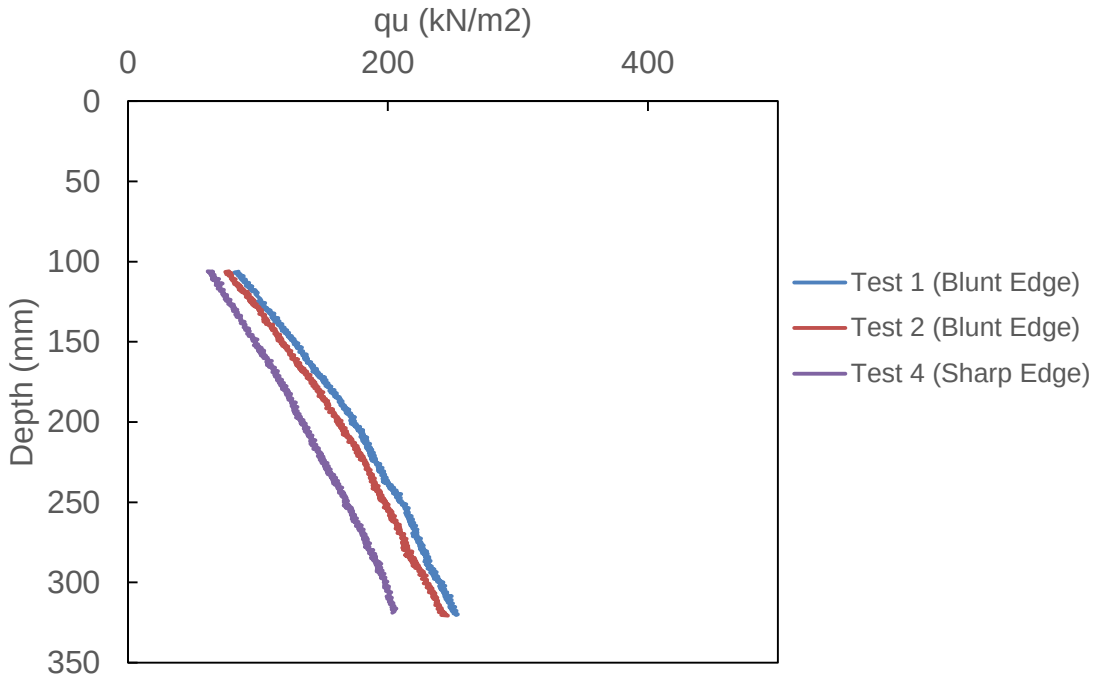

Figure 26: Bearing Stress over depth

Figure 26 shows a steady increase of the bearing stress over the depth. The curves can be described as linear with a slight parabolic shape.

In this research, the bearing stress was only calculated from the point of the anchor being fully embedded. The reason for this is that limitations in the measurement equipment and the uncontrolled behavior of the soil in terms of dilation cannot be seen as reliable.

With the measured data and the theoretical calculations the "true" bearing capacity factor N_q could be calculated. The bearing capacity factor is important for implementing it into the analytical model for predicting the embedment depth. It describes a factor which displays a relation from the bearing resistance and the depth and effective stress. The bearing capacity factor N_q is calculated by the following formula:

$$N_q(z) = \frac{q_u}{z * \gamma} \tag{26}$$

Where q_u is the bearing stress at a certain depth z and γ describes the effective stress of the soil.

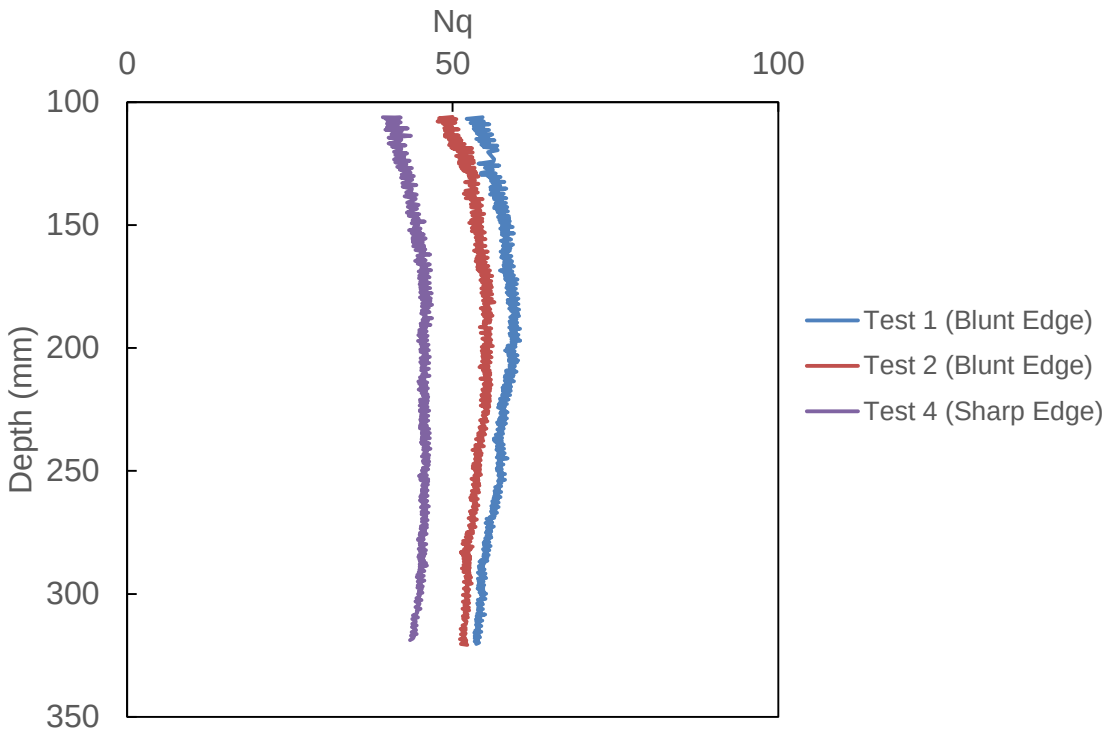

Figure 27: Depth *z* vs. Bearing Capacity Factor Nq for the static push test

The bearing capacity over the depth is plotted in Figure 27. Moreover, the first 105 mm are excluded in the calculation due to questionable reliability. The reason for this is that the Nq values being calculated vary extremely in the first 20 mm of penetration depth. This is mainly due to resolution of the instruments.

This figure shows that the bearing capacity factor has a minimum of 48 and a max of 60 for the blunt edge anchor and a minimum of 39 and a max of 47 for the blunt edge anchor.

The bearing capacity factor Nq has also been studied in the bearing capacity theory by Meyerhof (1951). Values for Nq for shallow footing were around 90 and the Nq value for

deep foundations regarding Meyerhof (1951) was 300. These values are significantly higher than the measured bearing capacity values.

DYNAMIC PENETRATION TESTS

The dynamic penetration tests were executed to understand the dynamic penetration behavior. Moreover, it was important to understand, which changes in the test set up and constants influence the penetration depth of the anchor. The following section will show, describe and explain the results from the dynamic penetration tests.

During the research, variables were identified. These were mainly the fall height, the shape of the anchor, either blunt or sharp edge shape, and the soil conditions, either saturated or dry condition. In addition to that, another variable was adding weight to the anchor, which is increasing the weight of anchor without changing its shape. (See Chapter 3 for more information and test set up description).

Table 2 presents a summary of the tests performed. The tests are numerated. The first number is displaying the test set up (e.g. the first test is a blunt edge anchor without adding weight penetrating in dry sand from a drop height of 2.7 meters). The second number is displaying the test number (e.g. 1.2 is displaying the second test of test set up 1).

Table 2: Summary of tests performed

Test	Anchor Shape	Soil Condition	Anchor Mass	Added Mass	Total Mass	Drop Height
			(kg)	(kg)	(kg)	(m)
1.1	Blunt edge	Dry	0.67	0.02	0.68	2.73
1.2	Blunt edge	Dry	0.67	0.02	0.68	2.68
2.1	Sharp edge	Dry	0.64	0.02	0.65	2.72
2.2	Sharp edge	Dry	0.64	0.02	0.65	2.73
3.1	Blunt edge	Dry	0.67	1.04	1.71	2.55
4.1	Sharp edge	Dry	0.64	1.08	1.71	2.49
5.1	Blunt edge	Dry	0.67	0.02	0.69	11.00
6.1	Blunt edge	Saturated	0.67	0.02	0.68	2.79
7.1	Blunt edge	Saturated	0.67	1.04	1.71	2.53

DYNAMIC PENETRATION TESTS IN DRY SAND

The dynamic penetration tests under dry conditions were executed for blunt and sharp edge anchors, with and without adding weight and one test from two different heights. The following table displays the tests that were executed under dry soil conditions.

Table 3: Penetration of blunt and sharp edge anchors

Test	Anchor Shape	Soil Condition	Anchor Mass	Velocity	Penetration	Penetration Angle
			(kg)	(m/sec)	(m)	
1.1	Blunt edge	Dry	0.68	7.32	0.13	5
1.2	Blunt edge	Dry	0.68	7.25	0.14	3
2.1	Sharp edge	Dry	0.65	7.31	0.15	15
2.2	Sharp edge	Dry	0.65	7.32	0.15	22
3.1	Blunt edge	Dry	1.71	7.08	0.28	4
4.1	Sharp edge	Dry	1.71	6.99	0.28	5
5.1	Blunt edge	Dry	0.69	14.69	0.16	72

The results in Table 3 show that the penetration depth (14.6cm) of a sharp edge anchor is slightly higher than the penetration depth of a blunt edge anchor (13.3 cm). In addition to that the penetration depth of a blunt edge anchor with double the speed resulted only in a slightly higher penetration depth (16.2cm). A significant difference between the blunt and sharp edge anchor was the penetration angle, which describes the angle at which the anchor was found after penetration. The penetration angle of the blunt edge anchor was on average 4 degrees, while the angle from the sharp edge anchor was on average 19 degrees. The test results suggest that the sharp edge anchor promotes tilting during the

flight. The blunt and sharped edge anchors at an impact velocity of 7.3 m/s penetrate between 1.23 to 1.39 times their fluke length.

Figure 28: Picture of the flight of the blunt edge anchor

Test 5.1, which had an impact velocity of 14.69 m/s, resulted in a really high penetration angle of 70 degrees. Looking at the picture which was taken during the flight (see Figure 28), the anchor already had a tilt during the flight. This could be one reason why the anchor penetrated into the soil at this angle. The results of test 5.1 are not included in further research, the anchor tilted highly during the flight. Its results are, therefore, not reliable.

The impact velocity of anchors with added weight, represented in Tests 3.1 and 4.1, was the same for both anchor types. Interestingly, while in the tests without adding weight the shape made a slight difference, the penetration depth is now the same with 0.28m or 2.6

times the anchor length for both anchor types (see chart). What this data shows, is that the anchor shape does not play an important role in terms of the same added weight. The penetration depth of both anchors is similar. The penetration angle, which has been significantly different from blunt to sharp edge anchors in the tests without added weight, does not play an important factor anymore and is similar as well (4 degree penetration angle vs. 5 degree penetration angle).

The penetration depths for the dry tests in general were varying between 1.23 and 2.6 times the anchor length. It seems that the penetration angle plays an important role in the tests without added weight, while in the tests with added weight there is no difference in the penetration angle and embedment depths for the two anchor shapes.

DYNAMIC PENETRATION TESTS IN SATURATED SAND

This section describes the results of two tests, both under saturated soil conditions. The difference of both tests is in the total anchor weight.

Table 4: Penetration of blunt edge anchor with and without adding weight in saturated conditions

Test	Anchor Shape	Total Anchor Weight	Drop Height	Velocity	Penetration	Penetration Angle	Soil Condition
		(kg)	(m)	(m/sec)	(m)		
6.1	Blunt edge	0.68	2.79	7.40	0.04	4	Saturated
7.1	Blunt edge	1.71	2.53	7.04	0.10	4	Saturated

The penetration of the anchor in a saturated sample can generally be described as low. Table 4 shows the impact velocity over the penetration depth of these tests.

The penetration depth of the blunt edge anchor without weight is 4.5 cm (1.75 in), which equals 0.4 times the fluke length, at an impact velocity of 7.4 m/s. The penetration depth of the blunt edge anchor with an added weight of 1.04 kg (2.3lb) was 10.5 cm, which equals around one times the fluke length of the anchor.

In both cases, the immediate penetration angle at the time of penetration was at around 4 degrees. At the point of impact, the anchor remains at that angle for a little bit, but then falls to one side and did not stay in the direction of penetration (see Figures 29 and 30).

Figure 29: Penetration of the blunt edge anchor at the moment of impacting into saturated sample

Figure 30: Final Position of the blunt edge anchor after penetrating into saturated sample

ANALYSIS OF THE DRAINAGE CONDITIONS DURING DYNAMIC PENETRATION

Soils can experience either drained or undrained conditions, depending on the rate of loading and the permeability of the soil. Coarse grained material, such as sands and gravels, can generally be described as drained, because of a high permeability. A low permeability soil such as silts and clays can be described as undrained.

Dry sand is obviously acting under drained conditions. Under saturated conditions, the question is, whether the soil is experiencing drained, partially drained or undrained conditions. To determine the drainage conditions, procedures which we know from Cone Penetration Tests (CPT) can be applied. Drainage conditions during penetration have already been analyzed for CPT in literature by Finnie and Randolph (1994). The authors came up with an equation which could determine whether a soil is experiencing undrained, drained or partially drained conditions under penetration.

$$V = vd_c/c_h \tag{27}$$

Where the dimensionless penetration rate V is calculated with the cone penetration rate v, the cone diameter d_c, and the coefficient of consolidation for lateral drainage. According to a number of researchers (Finnie and Randolph, 1994, Chung et al., 2006, Kim et al., 2008), the transition from fully undrained to partially drained conditions occurs when $V \approx 10$. (Bradshaw et al. 2012)

For this research and its tests, the findings have been applied for the saturated sands. As a cone penetration rate v the impact velocity of the anchor was taken, which was 7.3 m/s,

for the cone diameter d_c, the thickness of the anchor of 1.27 cm (0.5 inch) was taken. The coefficient of lateral drainage c_h was as calculated as a function of the coefficient of the vertical drainage, which is shown in the following:

$$c_h = c_v \frac{k_h}{k_v} \tag{28}$$

For simplicity reasons, the ratio of $\frac{k_h}{k_v}$ was taken as 1, which resulted in $c_h = c_v$. The coefficient of vertical drainage c_v was determined with the equation by Ranjan and Rao (2007).

$$c_v = \frac{k}{m_v \gamma_w} \tag{29}$$

Where k is the permeability index, m_v is the coefficient of volume compressibility and γ_w is the specific weight of water. A typical value for a loose sand for the coefficient of volume compressebility m_v was $1 * 10^{-4}\ kPa^{-1}$ from Domenico and Mifflin (1965). For the permeability index k a value of $5.1 * 10^{-4}\ {}^{cm}/_{s}$ from McCarthy (1998). A c_v of $51.99\ {}^{cm^2}/_{s}$ was calculated with equation 29 which is the same as c_h, which is calculated with equation 28.

The dimensionless penetration rate V was calculated with equation 27 and a value of 17.83 was the result. This shows by definition that the soil under penetration experiences undrained conditions. In addition to that, also the Handbook for Marine Engineering finds dynamic penetration in sands rapid enough that undrained conditions can be assumed. (NAVFAC, 2011)

DISCUSSION ON THE EXISTENCE OF BOUNDARY CONDITIONS

The effects of boundary conditions come into place due to the close distance of the penetrating anchor to the container wall. During penetration the influence zone of the penetrating anchor extends from the sand into the wall and therefore into the steel. Steel has a higher density and therefore also the strength of the soil is higher.

In literature Bolton et al. (1999) and Phillips & Valsangkar (1987) studied the effects in CPT tests in sands. They both tested the ratio S/B for sands, where S is the distance of the centre of the CPT test from the nearest container wall and B is the diameter of the cone. It was found that for a circular container, there is no significant deviation in Q, for both S/B = 11 and S/B = 22 (Bolton et al., 1999). Also Phillips & Valsangkar (1987), which have studied this ratio as well, recommend to maintain a ratio S/B > 10.

SUMMARY

Based on 1g model tests in dry and saturated sand the following summary points can be made:

- The penetration of the sharp edge anchor is higher than the blunt edge anchor for tests without adding weight to the anchor weight.
- The penetration of the sharp edge anchor is the same as the blunt edge anchor for tests with adding weight to the anchor weight. Furthermore, the final penetration angle was the same for both anchor shapes.
- The penetration depth in dry conditions is higher than the penetration depth in saturated conditions.

- It has been determined that anchors in dry conditions are penetrating under drained conditions while anchors in saturated conditions are penetrating under undrained conditions.

CHAPTER 5: NUMERICAL MODELING

Chapter 5 describes the development of two predictive numerical models that represent the drained tests under dry conditions based on the publication of Richardson et al. (2005) and for the undrained tests under saturated conditions based on the Handbook for Marine Geotechnical Engineering. Both of these approaches are described in Chapter 2 sections Richardson et al. (2005) and NAVFAC (2011).

The drained model, which was developed by Richardson et al. (2005), was applied to torpedo piles and a tri plate anchor developed by Dr. Aaron Bradshaw and Joseph Giampa. This model was extended in this thesis to predict the embedment for the kite shaped anchor as will be explained in the following sections.

The model is programmed in MATLAB, which is a multi-paradigm numerical computing environment that allows for matrix manipulations, plotting of functions and data, and implementation of algorithms.

MODELING DRAINED CONDITIONS IN DRY SAND

As mentioned above, the existing model has been used in previous research on torpedo piles and the triangular plates to predict the embedment as a function of velocity. Unfortunately Richardson et al. (2005) does not comment on whether they are dealing with drained or undrained conditions. This is the reason why it is assumed that they dealt with drained conditions. Therefore, this approach will be used for predicting the behavior of anchors in dry sand for drained conditions.

DEVELOPMENT OF THE MODEL

The publication and its formulas were already described in Chapter 2, but will be repeated here. Richardson et al. (2005) determined the static resistance force F_s as:

$$F_s = N_q \sigma_v' A_p + \beta \sigma_v' A_{shaft} \tag{30}$$

Furthermore, the embedment depth formula was introduced.

$$m \frac{d^2 z}{dt^2} = W_s - R_f \left(N_q \sigma_v' A_p + \beta \sigma_v' A_{shaft}\right) \tag{31}$$

where m is the anchor mass and R_f is a rate dependent term to account for velocity dependence of the soil resistance terms. R_f is further defined as:

$$R_f = (1 + \lambda \log \frac{v}{v_s}) \tag{32}$$

Where λ is a constant, v is the anchor velocity and v_s is the reference penetration velocity at which the static resistance was measured. Richardson et al. (2005) does not mention if they are dealing with drained, partially drained or undrained conditions.

Equation 31 was solved using the finite difference method by substituting $\dot{x}$ and $\ddot{x}$ with the following expressions

$$\dot{x} = \frac{x_i - x_{i-1}}{\Delta t} \tag{33}$$

$$\ddot{x} = \frac{x_{i+1} - x_i + x_{i-1}}{\Delta t^2} \tag{34}$$

Substituting equations 33 and 34 into equation 31 and rearranging yields.

$$\frac{m\, x_{i+1}}{\Delta t^2} = \frac{2\, m\, x_i}{\Delta t^2} - \frac{m\, x_{i-1}}{\Delta t^2} + W_s - (1 + \lambda \log \frac{x_i - x_{i-1}}{\Delta t}) \left(N_q \gamma z A_p + \beta \gamma \pi D x\right) \tag{35}$$

Solving equation 35 for x_{i-1} yields, this results in the following equation:

$$x_{i+1} = 2x_i + \frac{W_s\,\Delta t^2}{m} - x_{i-1} - \frac{\Delta t^2(1 + \lambda \log\frac{x_i - x_{i-1}}{\Delta t})\left(N_q \gamma x A_p + \beta\gamma\pi D x\right)}{m} \quad (36)$$

Assuming now a uniform and homogenous deposit, the only parameter for a torpedo pile that changes during the process of penetrating are A_p, the projected area, D, the diameter and obviously also the depth z. In this case, the A_p increased while the torpedo pile and especially its tip was fully penetrating into the soil. After that the value stays constant. Also the diameter D is increasing within the tip and after that staying constant over the length of the pile. The variable z is increasing with the increase in depth.

This model was fully programmed in MATLAB (Full Code in Appendix). Over the full length of the pile the same projected area A_p and diameter D was assumed. The full code of this model is attached in the appendix. Equation 36 is basically programmed with a for-loop where a number of elements, or basically how often the loop will be performed, is defined. Within this for-loop each embedment depth is calculated at a certain point following the for-loop with the formula described earlier. After that, the new velocity v is calculated with the following formula:

$$v(i) = \frac{(x_{i+1} - x_{i-1})}{2\Delta t} \quad (37)$$

After calculating embedment depth and velocity of the specific point the for-loop and therefore the if-loop starts again and continues until the final embedment depth is reached.

The model was then modified to match the requirements of a different shape and different soil specific parameters. The projected area A_p was programmed as constant over the

full length. Moreover, the shaft area A_{shaft} was applied to the actual are and the projected area was seen as constant over the full depth. In addition, the $N_q$value as well as the β value which are constants in the formula, were applied for the soil and anchor specifications. For the N_q values, the test results from the static push tests which were described in Chapter 4 can be used. The β value, which is the ratio of shaft friction to effective overburden stress, was also calculated from the corrected values described in Chapter 4. With the beta method which is known from deep foundation engineering, beta is calculated with the following formula:

$$\beta = K * \tan\delta \quad (38)$$

Where K can be calculated as $1.5 * K_0$ for piles (Conduto, 2001) and the interface friction angle δ is $^2/_3\,\phi'$. K_0 is defined as $1 - \sin\phi'$. An average beta of 0.28 was found over the full penetration depth.

The constants and the application for the kite shape were then programmed in the model. These were mainly parameters which describe the shape of the anchor, like length, width and thickness. Also, the weight of the anchor and the soil properties were applied. In addition to anchor shape parameters, the length from the edge to the greatest width was measured and defined. The rate dependent term R_f, which was applied in the publication from Richardson et al. (2005), was seen to be not applicable for dry tests. Sands do not seem to experience high strain rate effects in dry sands. Strain rate effects are believed to be negligible in dry sands. (e.g. Casagrande and Shanon, 1949, Sathialingam and Kutter, 1988) Therefore, the λ was assumed to be 0 in the calculation.

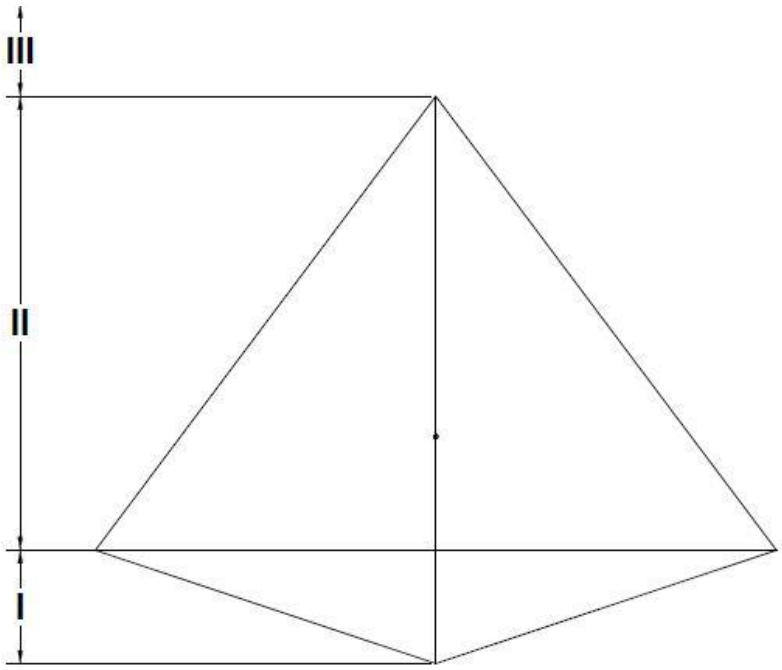

Figure 31: Anchor divided into Sections (I, II, III)

The if-loop which had only two cases in the existing model was extended to one extra case. The cases can be described as the following:

- The first case describes the depth from the edge to the greatest extent of the width (Area I in Figure 31)
- The second case describes the depth from the greatest extend of the width to the edge on the other side (Area II in Figure 31)
- The third case describes the fully embedded anchor (Area III in Figure 31)

Therefore, the anchor is basically divided into two big parts. The first is up to the depth where the width reaches a maximum and the other one is until the end of the anchor is reached.

Summarizing, the following simplifications were made

- The projected area is constant over the full length (including Area I)
- The bearing capacity factor N_q being constant over the full length
- The ratio of shaft friction to effective overburden stress β was assumed to be 0.28

As stated earlier the bearing capacity factor was calculated with the static penetration test. For the blunt edge the minimum Nq was 48, the max Nq was 60; therefore two different analysis for the max and the min case will be executed. Same will be for the sharp edge anchor with a minimum Nq of 39 and a maximum Nq of 46. The results of this sensitivity analysis are shown in the following.

SIMULATION OF THE MODEL TESTS

The result of the model is given in figure 32 as an example for a blunt edge anchor with a bearing capacity factor of 48. The model predicts the embedment depth as a function of velocity and shows therefore the change of velocity within the ground.

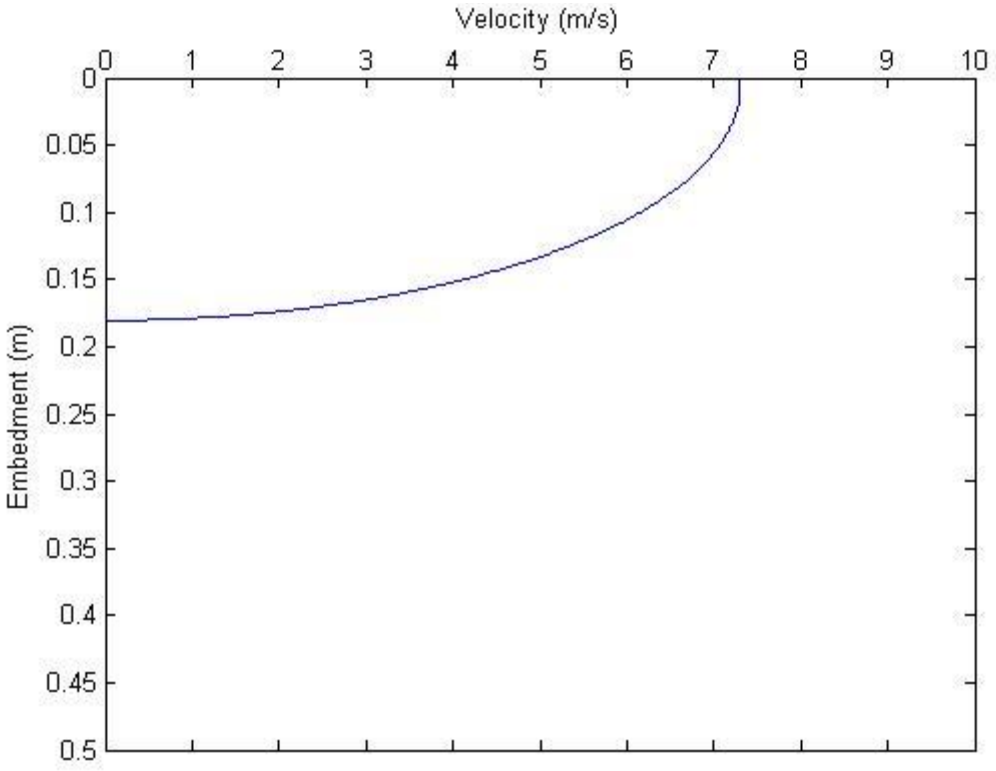

Figure 32: Results of drained Model for a blunt edge anchor without added additional weight for Nq of 48

Table 5: Comparison of predicted embedment depth and measured test results

Anchor Shape	Total Mass (kg)	Velocity (m/s)	Nq (-)	Beta	Depth (predicted)		Depth (measured)		Reference Test
					(m)	(H/B)	(m)	(H/B)	
Blunt edge w/o added weight	0.68	7.30	60 - 48	0.28	0.16 - 0.18	1.25 - 1.42	0.14	1.10	1.1; 1.2
Blunt edge w/ added weight	1.71	7.00	60 - 48	0.28	0.25 - 0.28	1.97 - 2.20	0.28	2.20	3.1
Sharp edge w/o added weight	0.65	7.30	46 - 39	0.28	0.18 - 0.19	1.42 - 1.50	0.15	1.18	2.1; 2.2
Sharp edge w/ added weight	1.71	7.00	46 - 39	0.28	0.29 - 0.31	2.28 - 2.44	0.28	2.20	4.1

The predicted results can definitely be described as close to the actual measured results. The model is slightly over-predicting the embedment depth, except for the blunt edge with adding weight. For the blunt edge, a bearing capacity factor should probably be closer to a value of 48 (min). Especially, the tests with a blunt edge anchor with adding weight seem to be more reliable. For the sharp edge anchor a bearing capacity factor of 46 (max) seem to have the best fit. This factor is generally over predicting the embedment depth but it can be considered as little comparing to lower bearing capacity factors.

What this table also shows, is that the bearing capacity factor has an important impact on the embedment depth, while the side friction as stated earlier, is only responsible for around 3 % of the total resistance. In other words, the anchor is mainly experiencing

bearing resistance. This explains why the bearing capacity factor plays this important role.

The presented measured and predicted data encourage a discussion and explanation of the soil behavior under dry conditions. Rapid loading tests have been made on dry sands and are reported in literature, with the result that the strain rate effect in dry sands is small or neglible. (e.g. Casagrande and Shannon, 1948) Although the behavior was studied later, rarely information is available on the change of friction angle during loading. Whitman (1970) reported that the friction angle for the tested sands first decreases as the strain rate increases beyond the required time to failure of 5 min. Later the trend reverses and a slight increase in strength is reported. Although the author questioned his results and indicated systematical errors as the explanation, Sathalingam and Kutter (1988) supported the findings by explaining this behavior with similar findings on bearing capacity reported by Vesic et al. (1965). The tests on bearing capacity show first a decrease in bearing capacity and as the loading velocity increases a gradual increase is reported.

MODELING UNDRAINED CONDITIONS IN SATURATED SAND

The model predicting the embedment depth of an anchor under saturated conditions will be described in the following section. The approach, which was used, was developed by the Handbook for Marine Geotechnical Engineering (2011), referred to as NAVFAC (2011). The authors assume an undrained soil condition, which means that the pore water in the soil does not have time to flow, and excess pore pressure are developed based on the soils' tendency for volume change (NAVFAC, 2011).

Therefore, this approach will be used for predicting the behavior of scaled anchors in saturated sand for undrained conditions, as well as predicting the anchor behavior for the full scale.

DEVELOPMENT OF THE MODEL

The publication NAVFAC (2011) and its formulas were already described in Chapter 2, but will be repeated here. The authors developed an embedment prediction model for penetrating objects into the seabed under undrained conditions. Different forces acting on the penetrating object are introduced. These are shown in the formula below. A positive force describes a downward and a negative force describes a resisting or upward force.

$$F_i = F_{di} + W_{bi} - Q_{ni} - F_{si} - F_{hi} \tag{39}$$

Where F_i is the net total downward force, F_{di} is the external driving force (e.g. rocket motor), W_{bi} is the penetrator buoyant weight, Q_{ni} is the nose or tip bearing resistance, F_{si} is the side friction or adhesion and F_{hi} is the fluid drag force.

The tip resistance can be determined as

$$Q_{ni} = S_{ui}(nose) S_{\dot{e}i} N_{ti} A_t \tag{40}$$

Where $S_{ui}(nose)$ is the soil undrained shear strength at a depth 0.35 B below z, averaged over ith increment of penetration, $S_{\dot{e}i}$ is the strain rate factor, A_t is the end area of penetrator and N_{ti} is a dimensionless nose resistance factor, which is determined by the following formula.

$$N_{ti} = N_c' = [(2+\pi)]\left[1 + \left(\frac{1}{2+\pi}\right)\left(\frac{B}{L}\right)\right][1 + \left(\frac{2}{2+\pi}\right)\arctan\left(\frac{D_f}{B}\right)] \tag{41}$$

The soil undrained shear strength is determined with

$$S_{ui}(nose) = \left[\frac{\sigma_{cr}\left(N_{\phi} - 1\right)}{2}\right] \tag{42}$$

Where σ_{cr} is the critical confining stress, and N_{ϕ} is a bearing factor.

The side friction F_{si} is determined with

$$F_{si} = \left[\frac{S_{ui}\,(side)}{S_{ti}}\right] S_{\dot{e}\imath} A_{si} \tag{43}$$

Where S_{ui} is the soil undrained shear strength averaged over the length of the penetrator in contact with the soil, A_{si} is the side soil contact area of the penetrator, S_{ti} is the soil sensitivity. In cohesionless soils, such as sands, we usually do not deal with issues of sensitivity. In this context, it makes therefore sense to think of a substitute of this parameter for sands.

$$S_{\dot{e}\imath} = \frac{S_{\dot{e}}^{*}}{1 + [\frac{C_{\dot{e}} v_i}{S_{ui} D_e} + C_0]^{-0.5}} \tag{44}$$

Where $S_{\dot{e}}^{*}$ is the maximum strain rate factor, $C_{\dot{e}}$ is the empirical strain rate coefficient, v_i is the velocity at a certain depth, C_0 is the empirical strain rate constant, S_{ui} is the undrained shear strength and D_e is the equivalent diameter of penetrator.

The authors also include a fluid drag force in their equation. This formula seems to be reasonable, while the object is moving through the water. The authors assume that this force will continue as it moves through the soil. This force is calculated by the following formula:

$$F_{hi} = (0.5) C_D \rho A_t (v_i)^2 \tag{45}$$

Where C_D is the dimensionless fluid drag coefficient, which is the same as that in seawater, ρ is the mass density of the soil, the "fluid" being accelerated and v_i is the penetrator velocity after penetrating the ith layer.

It is somehow questionable, whether this force should be included while the anchor is penetrating through the soil, especially since the other forces are already including parameters accounting for drag forces in the soil. From a theoretical point of view, this force should be included for the area which will be above the soil surface at the point of initial penetration. Including and excluding this term in later calculation, it was seen that this term does not have a big impact on the penetration depth. In the following, this term should, therefore, be neglected.

The model uses the formulas which were described earlier. As a model of solution, a finite difference solution analog to the drained model was used. The following theoretical steps were developed in order to develop a code which can be programmed into MATLAB (Full Code in Appendix).

$$m\ddot{x} - W' + S_u\, S_{\dot{e}\imath}(\dot{x}) N_{ti}(\dot{x}) A_t + S_u\, S_{\dot{e}\imath}(\dot{x}) A_s = 0 \tag{46}$$

By substituting $\dot{x}$ and $\ddot{x}$ with the following expressions

$$\dot{x} = \frac{x_i - x_{i-1}}{\Delta t} \tag{47}$$

$$\ddot{x} = \frac{x_{i+1} - x_i + x_{i-1}}{\Delta t^2} \tag{48}$$

a further developed formula can be expressed by substituting and rearranging

$$\frac{m\,x_{i+1}}{\Delta t^2} = \frac{2\,m\,x_i}{\Delta t^2} - \frac{m\,x_{i-1}}{\Delta t^2} + W' - S_u\,S_{\dot{e}\iota}(\dot{x})N_{ti}(\dot{x})A_t + S_{ur}S_{\dot{e}\iota}(\dot{x})A_s \qquad (49)$$

The goal is it now to rearrange the equation towards x_{i-1}. Eventually, this results in the following equation. Due to simplicity the substitutions of $\dot{x}$ are not written in this formula.

$$x_{i+1} = 2x_i + \frac{W'\Delta t^2}{m} - x_{i-1} - \frac{\Delta t^2 S_u\,S_{\dot{e}\iota}(\dot{x})N_{ti}(\dot{x})A_t + S_{ur}\,S_{\dot{e}\iota}(\dot{x})A_s}{m} \qquad (50)$$

What the equation indicates is the $S_{\dot{e}\iota}$ and N_{ti} are dependent on the velocity, or specifically on the embedment depth over the increment of time Δt.

With the equation, the embedment depth x_{i+1} in every point can be calculated and, therefore, the velocity v can also be calculated with the following formula:

$$v(i) = \frac{(x_{i+1} - x_{i-1})}{2\Delta t} \qquad (51)$$

Similar to the drained model, the constants and the application of the kite shape were programmed in the undrained model. These were mainly parameters which describe the shape of the anchor, like length, width and thickness. Also the weight of the anchor was applied.

In the MATLAB model equation 50 is basically programmed with a so called for-loop where a number of elements, or basically how often the loop will be performed, is

defined. Within this for-loop the model is calculating each embedment depth at a certain point.

The if-loop is as well as the if loop for the drained model divided into three different cases. The cases are analog to the ones of the drained model:

Besides the changing area, which is crucial for accounting for the side friction, the model implies further features which will be explained in the following: The buyout weight which is the anchor dry weight subtracted by the buyout force, is changing over the depth. Furthermore, the dimensionless nose resistance factor, $N_{ti}$is calculated for every increment in time and is therefore also applied to every embedment depth and velocity. The same applies for the strain rate factor $S_{\dot{e}i}$, which consists of three parameter values:

- $C_{\dot{e}}$ (the empirical strain rate coefficient)
- $S_{\dot{e}}^{*}$ (the maximum strain rate factor)
- C_0 (the empirical strain rate constant)

These values were determined from the chart presented in NAVFAC (2011). For objects where excess penetration is of primary concern, the value for $S_{\dot{e}}^{*}$ is 2, for $C_{\dot{e}}$ is 1915.2 N/m2 and C_0 is 1.0.

The undrained shear strength seemed to be a difficult property to measure. When sands are sheared during a dynamic penetration event, the pore water pressure does not have time to flow, and failure occurs when either the sand grains are crushed or cavitation of the pore water occurs. Dealing with this problem, Seed and Lee (1967) developed

methods to predict the undrained shear strength from drained data. Result of this is the calculation of the undrained shear strength with the following formula:

$$S_u = \left(\frac{\sigma_{cr}\left(N_\phi - 1\right)}{2}\right) \tag{52}$$

To determine the critical confining stress and the fractional relative density equations 12 and 13 were used. A critical confining stress for the saturated sample, with a unit weight of 19.49 and a critical state friction angle of 33.4, of 246.4 kPa was estimated with a fractional relative density of 0.45. The undrained shear strength of S_u was then calculated with a calculated N_ϕ of 3.45 from equation 14 and the critical confining stress and resulted in a value of 301.7 kPa. In addition to this approach, results were also determined for an undrained shear strength of 15 kPa as a reference value.

In addition to that, it was assumed that shearing of the sample results in only dilative behavior and no strain softening has occurred. In this case the residual load S_{ur} is the same as the undrained shear strength S_u. Usually, the relation can be described as

$$S_{ur} = c * S_u \tag{53}$$

Where c varies between 0 and 1. (see also Yoshemi et al., 1999)

SIMULATION OF THE MODEL TESTS

The result of the model is given in figure 33, as the velocity over embedment depth for a blunt edge anchor without adding weight as an example for an undrained shear strength of 15 kPA.

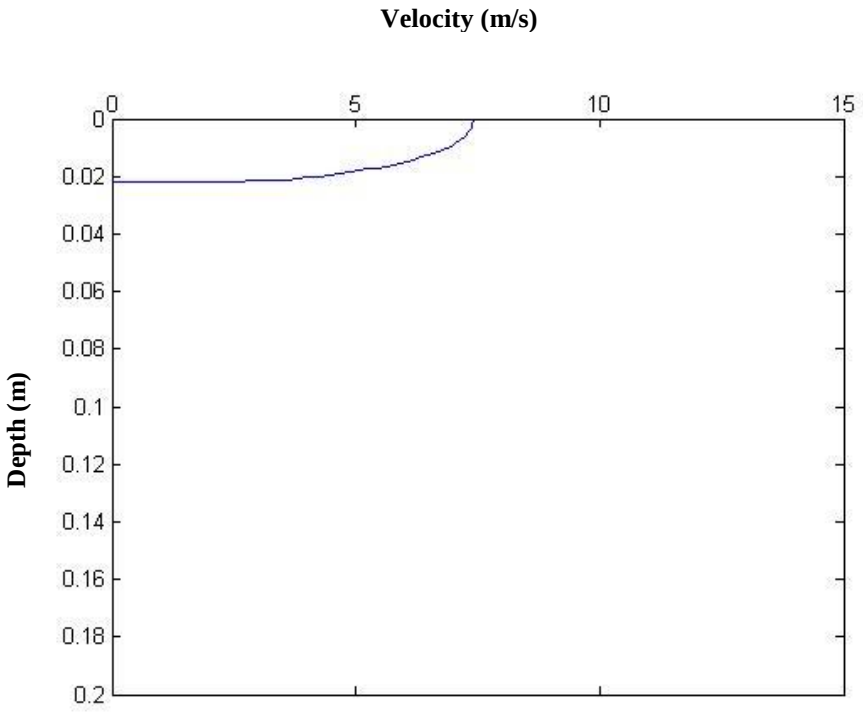

Figure 33: Velocity over embedment depth for the Blunt edge anchor with Su = 302 kPa

Table 6 compares the predicted and actual measured results at different undrained shear strengths for the blunt edge anchor with and without adding weight.

Table 6: Comparison of predicted embedment depth and measured test results

Anchor Shape	Total Mass (kg)	Velocity (m/s)	Su (kPa)	Depth (predicted)		Deapth (measured)		Reference Test
				(m)	(H/B)	(m)	(H/B)	
Blunt edge w/o added weight	0.68	7.30	302 - 15	0.022 - 0.068	0.17 - 0.54	0.044	0.35	6.1
Blunt edge w/ added weight	1.71	7.00	302 - 15	0.027- 0.122	0.21 - 0.96	0.105	0.83	7.1

From the data it is obvious that at an undrained shear strength of 302 kPa the model is under-predicting the embedment depth for the blunt edge with and without added weight.

As a second reference, undrained shear strength of a value of 15 kPa had a good agreement with the measured data. While the model in this case is slightly over-predicting the embedment depth of just the anchor, the anchor with adding weight is almost on point the same value. This shows clearly that the undrained shear strength, which is a difficult parameter to estimate, has a crucial effect on predicting the embedment depth and the reliability of the model.

Saturated sand under rapid loading is highly influenced by volume change tendency in shear. Under static or slow loading, loose sands tend to compress and dense sands tend to dilate. (Omidvar et al., 2012) Dilation results in a decreasing pore water pressure and increasing effective stress, while contraction results in an increasing pore water pressure and decreasing effective stress. Under rapid loading, loose saturated sands tend to dilate. Whitman (1970) reported an increase in the soil of 200% at low to moderate confining pressures. If the decrease in pore water pressure is high enough, the pore water will cavitate.

The described behavior can be displayed in the presented tests. The saturated sand sample built up high strength. The sand sample, tended to dilate with the effect of decreasing pore water pressure and increasing strength. Comparing the embedment depth from the blunt edge anchor under dry and saturated soil conditions, a difference of factor 3 is reported. This agrees with Whitman (1970). In this context it is not sure if cavitation occurs, which would limit the pore water pressure to -1 atm.

PREDICTIONS FOR THE FULL SCALE ANCHOR

As discussed earlier, the sand was seen to experience dilation during the penetration of the anchor. This behavior can be assumed as long as the confining pressures are assumed to be low. Dilation occurs as long as the effective stress paths increase and q, so the $\frac{\sigma_1-\sigma_3}{2}$, increases to the value of the residual undrained shear strength. Good agreement with the measured data and the predicted data was achieved with an undrained shear strength of 15 kPa. If the soil remains dilative at the prototype scale at the same void ratio, 15 kPa should be a reasonable estimate of the undrained shear strength of the full-scale anchor.

If the soil in the prototype is contractive due to the higher confining pressures, the peak undrained shear strength will be higher than 15 kPa. The strength in the prototype was therefore modeled using the equations proposed by Seed and Lee (1967) that resulted in an undrained shear strength of 302 kPa.

The results of the model are shown in Table 8.

Table 7: Predicted embedment depth for Full Scale Anchor

Anchor Shape	Total Mass (t)	Velocity (m/s)	Su (kPa)	Depth (predicted)	
				(m)	(H/B)
Full Scale	47	7.50	302 - 15	1.16 - 7.78	0.23 - 1.53
		13.0	302 - 15	1.88 - 10.01	0.37 -1.99
		24.0	302 - 15	3.34 - 14.38	0.66 - 2.83

The impact velocities of 7.5 m/s, 13 m/s and 24 m/s were carefully chosen to match with the impact velocities which were published for torpedo piles, mainly by Richardson et al. (2005) and Madeiras (2002).

The embedment depths vary and are dependent on the impact velocity and undrained shear strength. For an impact velocity of 7.5 m/s the embedment depth varies between 1.16 m (for Su = 302 kPa) and 7.78m (for Su = 15 kPa). For an impact velocity of 13 m/s the predicted depth is 1.88m (for Su = 302 kPa) and 10.01m (for Su = 15 kPa). For an impact velocity of 24 m/s the predicted depth is 3.08m (for Su = 302 kPa) and 8.70m (for Su = 15 kPa). Madeiras (2002) reported embedment depth of 1.5 times the anchor length for a test at an impact velocity of 24 m/s. Richardson et al. (2005) reported 0.7 times the anchor length for an impact velocity of 7.5 m/s and 0.9 times the anchor length for an impact velocity of 13.0 m/s. Both authors tested the anchor in calcareous sands. These values are within the range of depth predicted from the undrained model.

In the full scale tests the importance of the correct estimation or better determination of the undrained shear strength is obvious. Although the reported test data is within the ranges given by the undrained model, these ranges are huge and, therefore, do encourage further study. Future research should, therefore, focus on analyzing strain rate effects of saturated sands as well as better predication models of undrained shear strength and undrained shear strength at the critical state.

CHAPTER 6: CONCLUSIONS

The topic of this thesis was the investigation of the penetration behavior of the "Flying Wing Anchor" (patent pending). The penetration behavior of objects in sand have already been studied previously. The literature review is displaying relevant literature in this field, along with physical tests and first prediction models for the embedment depth.

The goal of this thesis, to investigate and analyze the behavior under dynamic penetration in sand, was accomplished through a combination of 1g model experiments and numerical modeling. The physical tests led to the following findings:

- The penetration of sharp edge anchors is higher than the blunt edge anchor for tests without adding weight to the anchor weight.
- The penetration of the sharp edge anchors is the same as the blunt edge anchor for tests with adding weight to the anchor weight. Furthermore, the final penetration angle was the same for both anchor shapes.
- The penetration depth in dry conditions is higher than the penetration depth in saturated conditions.
- It has been determined that anchors in dry conditions are penetrating under drained conditions while anchors in saturated conditions are penetrating under undrained conditions.

The analytical modeling used the in the literature review introduced prediction formulas along with the results being measured by the physical tests to construct and program a embedment prediction model. In this context, two different models were developed:

1. Model for Drained Conditions
2. Model for Undrained Conditions

While the first model predicts embedment depths for dynamic penetration in dry sand, the second model predicts embedment depth for dynamic penetration in saturated sand. The second model was further applied in a full scale prediction model of the Flying Wing Anchor.

The feasibility of the concept has been shown by prediction depths of approximately up to 3 times the fluke lengths for impact velocities of 24 m/s which were achieved in physical field tests (see Madeiras, 2002).

This research further underlines the effect of contraction and dilation of saturated soils. Especially, the effect of dilation with decrease in pore water pressure and increase in effective stress for the saturated tests of saturated sand samples can be well seen from the findings of this research.

Further research is encouraged in the soil behavior of saturated sands under rapid loading. Although more recently research has been touching this topic, the change in pore water pressure is still unknown, especially for dense sand. (Omidvar et al., 2012) Evaluating more data would help to understand and predict the effect of saturation on rapid loading better.

CHAPTER 7: REFERENCES

ASTM Standard (2006a) "Test methods for Maximum Index Density and Unit Weight of Soils Using Vibratory Table", ASTM International, West Conshohocken, PA, DOI: 10.1520/D4253-00R06

ASTM Standard (2006b) "Test methods for Minimum Index Density and Unit Weight of Soils and Calculation of Relative Density", ASTM International, West Conshohocken, PA, DOI: 10.1520/D4254-00R06E1

Bishop, A.W. and Eldin, A. K. G.(1953); "The Effect of Stress History on Relation between ϕ and Porosity of Sand", Proceedings, 3rd International Conference on Soil Mechanics and Foundation Engineering, Vol. I, pp. 100 – 105.

Bolton, M.D. (1986) "The Strength of Dilatancy of Sands", Geotechnique, Vol. 36, No. 1, pp. 65-78.

Bolton, M. D., Gui, M. W., Garnier, J., Corte, J. F., Bagge, G., Laue, J. and Renzi, R. (1999): "Centrifuge cone penetration test in sand", Géotechnique, Vol. 49, No. 4, pp. 543-552.

Bradshaw, A.S., Moralez-Velez, A.C., Baxter, C.P.D. (2012): "Evaluation of Existing CPT Correleations in Silt", Geotechnical Engineering Journal of the SEAGS & AGSSEA, Vol. 43 No. 4, pp. 1 – 10.

Bradshaw, A.S., Giampa, J., Dietrich, F., Gilber, R. and Gerkus, H. (2015) “Pullout capacity of plate anchors in sand for floating offshore wind turbines.” Frontiers in Offshore Geotechnics III.

Butterfield, C.P., Musial, W. and Jonkman J. (2007) “Overview of Offshore Wind Technology: Preprint”, NREL.

Butterfield, R. and Adrawes, K.Z. (1970) “An Air Activated Sand Spreader for Forming uniform Sand Beds”, Geotechnique, 20(1), pp. 97 – 100.

Casagrande, A. and Shannon, W. L. (1949). "Strength of Soils under Dynamic Loads", Transactions, ASCE, Vol. 114

Chung, S.F., Randolph, M.F. and Schneider, J.A. (2006): “Effect of penetration rate on penetrometer resistance in clay,” Journal of Geotechnical and Geoenvironmental Engineering, ASCE, 132(9), pp. 1188 – 1196.

Conduto, D. P. (2001) “Foundation design: principles and practices”, Prentice Hall, Upper Saddle River, New Jersey

Dave, T. N. and Dasaka, S. M. (2012), “Assesment of portable traveling pluviator to prepare reconstituted sand specimens.” Geomechanics and Engineering – An International Journal, 4 (2), 79-90.

Dietrich, F. (2014). “Evaluation of Theoretical Capacity Models for Plate Anchors in Sand in Relation to Floating Offshore Wind Turbines.” Masterthesis at University of Rhode Island, Kingston, Rhode Island.

Finnie, I.M.S. and Randolph, M.F. (1994): “Punch-through and liquefaction induced failure of shallow foundations on calcareous sediments,” Proceedings of the 17th International Conference on the Behavior of Offshore Structures, Massachusetts, USA, 1, pp. 217 – 230.

Gade, V.K., Dave, T.N., Chauhan, V.B. and Dasaka, S. (2013) “Portable Traveling Pluviator To Reconstitute Specimens of cohensionless Soils.” Proceedings of Indian Geotechnical Conference, pp. 1 - 12

Gaudin, C., O’Loughlin, C. D., Randolph, M. F. and Lowmass, A. C. (2006), “Influence of the installation process on the performance of suction embedded plate anchors” Géotechnique 56, No. 6, 381–391

Giampa, J.R. (2014) “Interpretation of Shallow Helical Anchor Capacity in Sand”. Masterthesis, University of Rhode Island, Kingston, Rhode Island.

Gilbert, R. and Bradshaw, A.S., (2012); Green Foundations for Green Energy. Research Proposal submitted to the National Science Foundation.

Kim, K., Prezzi, M., Salgado, R., Lee, W. (2008). “Effect of penetration rate on cone penetration resistance in saturated clayey soils” Journal of Geotechnical and Geoenvironmental Engineering, ASCE, 134 (8), pp. 1142 – 1153.

Le Lievre, B., and Tabatabaee, J. (1981); The performance of marine anchors with planar flukes in sand; Canadian Geotechnical Journal, 18, pp. 520-534

Lieng, J.T., Hove, F. and Tjelta, T.I. (1999); Deep penetrating anchor: Subseabed deepwater anchor concept for floaters and other installation. Proc. 9th International Offshore and Polar Engineering Conf., Brest, France 1, pp. 613 – 619

Liu, H., Li, Y., Yang, H., Zhang, W., and Liu, C. (2010a); Analytical study on the ultimate embedment depth of drag anchors. Ocean Engineering, 37(14-15), 1292-1306.

Liu, H., Zhang, W., Zhang, X., and Liu, C. (2010b); Experimental investigation on the penetration mechanism and kinematic behavior of drag anchors. Appl. Ocean Res. 32 (4), pp. 434-442.

Matha, D., Fischer, T. and Kuhn, M. (2009) “Model Development and Loads Analysis of a Wind Turbine on a Floating Offshore Tension Leg Platform”

McCarthy, David F., (1998) “Essentials of Soil Mechanics and Foundations: Basic” Geotechnics, Fifth Edition, Prentice Hall.

Medeiros, C. J. Jr. (2001), “Torpedo Anchor for Deep Water” , DOT Conference, Rio de Janeiro, Oct. 2001.

Medeiros, C. J. Jr. (2002); Low cost anchor system for flexible risers in deep water. Offshore Technology Conference OTC 14151, pp. 1 – 5

Meyerhof, G. G. (1951); The Ultimate Bearing Capacity of Foundations, Géotechnique, Volume 2, Issue 4 pp. 301 –332

Rocker, K., Thompson, D., Jung, B., Briaud, J., Lin, S. (2011); Handbook for Marine Geotechnical Engineering. Naval Facilities Engineering Command (NAVFAC)

Okamoto, M. and Fityus, S. (2006) “An evaluation of the dry pluviation preparation technique applied to silica sand samples” Geomechanics and Geotechnics of Particulate Media, pp. 33-39

O’Loughlin, C.D., Randolph, M.F. and Richardson, M.D. (2004) “Experimental and Theoretical Studies of Deep Penetrating Anchors” Proc. Offshore Technology Conference, Houston, Texas, USA.

Omidvar, M., Iskander, M., Bless, S. (2012) “Stress-Strain behavior of sand at high strain rates”, International Journal of Impact Engineering, Vol. 49, pp. 192 – 213.

Prezzi, M. (2009) ‘Implementation of Laterally Loaded Piles in Multi-Layer Soils’. Purdue University, West Lafayette, Indiana..

Phillips, R. and Valsangkar, A. (1987): “An experimental investigation of factors affecting penetration resistancein granular soils in centrifuge modelling,” CUED/DTR210. 17p.

Ranjan, G. and Rao, A.S.R. (2007): “Basic and Applied Soil Mechanics,” New Age International.

Raie, M.S., and Tassoulas, M. (2009); Installation of Torpedo Anchors: Numerical Modeling. Journal of Geotechnical and Geoenvironmental Engineering ASCE: 1805 – 1813.

Richardson, M.D., O’Loughlin, C.D., Randolph, M.F. (2005); The geotechnical performance of Deep Penetrating Anchors in calcareous sand. Frontiers in Offshore Geotechnics, London, UK: 357 – 363

Sathialingam, N. and Kutter, B. L. (1988) “The effects of high strain rate and high frequency loading on Soil Behavior in centrifuge model tests”, University of California, Naval Civil Engineering Laboratory.

Seed, H. B. and Lee, K. L. (1967) “Undrained Strength Characteristics of Cohesionless Soils”, Journal of the Soil Mechanics and Foundation Division, Procedings of the American Society of Civil Engineers, Vol. 93, No. SM6, November 1967

Snyder, B. and Kaiser, M.J. (2009) “Ecological and economic cost-benefit analysis of offshore wind energy”, Renewable Energy, Vol. 34, No. 6, pp.1567–1578.

Sridharan, A. and Nagaraj, H.B. (2004) “Coefficient of Consolidation and its Correlation with Index Properties of Remolded Soils”, Geotechnical Testing Journal, Vol. 27, No. 5, pp. 1 – 6.

TU Delft; M. van den Hatert, B. Jonkman, D. Strijbis (2005); Penetration behavior of an anchor in sand.

Vesic, A. S., Banks, D. C. and Woodward, J.M. (1965), “An Experimental Study of the dynamic Bearing Capacity of Footings on Sand”, Proceedings of the 6th International Conference of the Soil Mechanics and Foundation Engineering, Vol. 2, pp. 209 - 213

Whitman, R.V. (1970) “The Response of Soils to Dynamic Loadings; Report No. 26, Final Report’, Contract Report No. 3-26, U.S. Army Engineer Waterways Experiment Station, Corps of Engineers, Vicksburg, Mississippi

Wilde, B., Treu, H. & Fulton, T. (2001). Field testing of suction embedded plate anchors. Proc. 11th International Offshore and Polar Engineering Conference, Stavanger, 544–551.

Yoshimine, M., Robertson, P.K. and Wride, C.E.(1999), “Undrained shear strength of clean sands to trigger flow liquefaction”, Canadian Geotechnical Journal, Vol. 36, pp. 891–906